



**HAL**  
open science

## Hydrogel foams from liquid foam templates: Properties and optimisation

I. Ben Djemaa, S. Auguste, Wiebke Drenckhan-Andreatta, S. Andrieux

► **To cite this version:**

I. Ben Djemaa, S. Auguste, Wiebke Drenckhan-Andreatta, S. Andrieux. Hydrogel foams from liquid foam templates: Properties and optimisation. *Advances in Colloid and Interface Science*, 2021, 294, pp.102478. 10.1016/j.cis.2021.102478 . hal-03476586

**HAL Id: hal-03476586**

**<https://hal.science/hal-03476586v1>**

Submitted on 2 Aug 2023

**HAL** is a multi-disciplinary open access archive for the deposit and dissemination of scientific research documents, whether they are published or not. The documents may come from teaching and research institutions in France or abroad, or from public or private research centers.

L'archive ouverte pluridisciplinaire **HAL**, est destinée au dépôt et à la diffusion de documents scientifiques de niveau recherche, publiés ou non, émanant des établissements d'enseignement et de recherche français ou étrangers, des laboratoires publics ou privés.



Distributed under a Creative Commons Attribution - NonCommercial 4.0 International License

# Hydrogel foams from liquid foam templates: properties and optimisation

I. Ben Djemaa<sup>1,2</sup>, S. Auguste<sup>2</sup>, W. Drenckhan-Andreatta<sup>1</sup>, S. Andrieux<sup>2</sup>

<sup>1</sup> Institut Charles Sadron, University of Strasbourg, CNRS UPR22, 23 rue du Loess, 67037 Strasbourg, France

<sup>2</sup> Urgo Research Innovation and Development, 42 rue de Longvic, 21304 Chenôve Cedex

## Abstract

Hydrogel foams are an important sub-class of macroporous hydrogels. They are commonly obtained by integrating closely-packed gas bubbles of 10-1000 micrometres into a continuous hydrogel network, leading to gas volume fractions of more than 70% in the wet state and close to 100% in the dried state. The resulting wet or dried three-dimensional architectures provide hydrogel foams with a wide range of useful properties, including very low densities, excellent absorption properties, a large surface-to-volume ratio or tuneable mechanical properties. At the same time, the hydrogel may provide biodegradability, bioabsorption, antifungal or antibacterial activity, or controlled drug delivery. The combination of these properties are increasingly exploited by a wide range of applications, including the biomedical, cosmetic or food sector. The successful formulation of a hydrogel foam from an initially liquid foam template raises many challenging scientific and technical questions at the interface of hydrogel and foam research. Goal of this review is to provide an overview of the key notions which need to be mastered and of the state of the art of this rapidly evolving field at the interface between chemistry and physics.

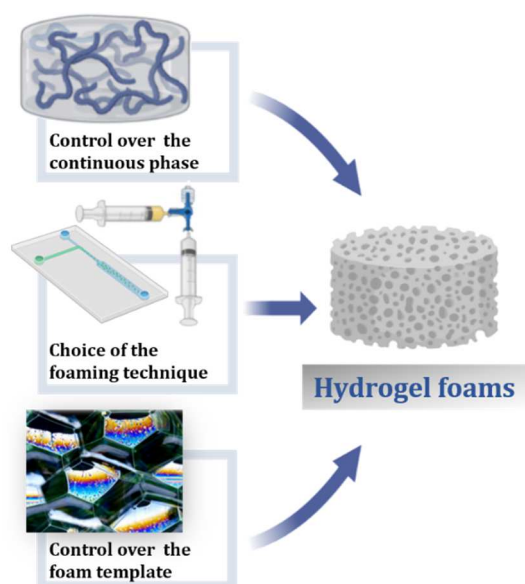


## Table of Contents

1. Introduction .....	3
2. Control over the liquid foam template .....	5
2.1. Introduction .....	5
2.2. Controlling the liquid foam structure .....	6
2.3. Maintaining the gas fraction: foam drainage .....	6
2.4. Maintaining foam shape: foam flow under gravity .....	8
2.5. Maintaining the bubble size: coalescence and coarsening.....	9
3. Control over the continuous hydrogel phase .....	13
3.1. Classification of hydrogels .....	13
3.2. Nature of cross-links .....	13
3.3. Kinetics of gelation.....	17
4. Hydrogel foams from liquid foam templates.....	18
4.1. Chemical foaming .....	18
4.2. Physical foaming .....	23
4.2.1. Mechanical foaming.....	23
4.2.2. Foaming by gas injection.....	25
4.2.2.1. Batch foaming .....	25
4.2.2.2. Microfluidic foaming .....	28
5. Selected properties of hydrogel foams.....	31
5.1. Porosity and pore size.....	31
5.2. Shear modulus .....	32
5.3. Pore connectivity .....	33
5.4. Absorption capacity of hydrogel foams.....	35
6. Conclusion.....	37
7. Acknowledgement .....	38
8. References .....	38

**Keywords:** hydrogel foams; hydrogels; liquid-foam templating; biomedical materials

## 1. Introduction

Hydrogel foams are a specific class of macroporous materials [1] in which the dispersed phase is a gas, and the continuous phase is a hydrogel. Hydrogel foams are of great importance in many different areas, the most popular being the biomedical, sanitary, food or agricultural sectors. In the biomedical sector, for example, they are used as scaffolds for cell growth and tissue engineering [2–4], wound dressings [5,6], or encapsulation [7]. These applications commonly exploit a combination of the three-dimensional pore network, the large surface-to-volume ratios, the low densities and tuneable mechanical properties. The advantage of using hydrogels, rather than other polymers, is their elastic and flexible structure, their high biocompatibility, ease of incorporating therapeutic molecules within their network, their stimuli-responsive features or their ability to combine the properties of different polymers (e.g., mixing swellable polymers with a stimuli-responsive polymer) [8].

Each specific application imposes its own constraints on the porous architecture of the hydrogel foam. The main architectural parameters that must be controlled are the pore-size distribution, the porosity and the connectivity of neighbouring pores. Moreover, each application requires a specific choice of the material composing the hydrogel. Frequent criteria for this choice include temporal stability, the need for biocompatible and/or bioabsorbable polymers, non-irritant formulations, an antifungal and antibacterial activity, a low toxicity or a strong absorption capacity. Therefore, one needs to finetune both the properties of the hydrogel itself and the structure of the foam to generate efficient hydrogel foams with the desired properties and functionalities. The challenge in making hydrogel foams is thus the combination of these two levels of control, requiring closer interaction between scientific communities specialised in the formulation of hydrogels and specialised in foam research. This review, therefore, aims to establish a bridge between both communities.

To refine the definition of a hydrogel foam given above, let us make the distinction between hydrogel foams and macroporous hydrogels. Macroporous hydrogels are a broad definition of porous materials in which gas is dispersed in a hydrogel matrix, “macroporous” indicating pores larger than 50 nm [9]. Macroporous hydrogels with interconnected pores are also sometimes called “superporous hydrogels” (SPH) [10]. Hydrogel foams are a sub-group of macroporous hydrogels which contain enough gas so that the pores touch each other. For narrow pore size distributions, this is reached at porosities above 64%. I.e., all hydrogel foams are macroporous hydrogels, but not all macroporous hydrogels are hydrogel foams. Beyond the porosity, it is their structure that makes the specificity of hydrogel foams. Pore sizes are commonly larger than 10 micrometres and the pore shapes are dictated by surface tension effects in the liquid state. Hydrogel foams are thus made via the gelation of an initially liquid foam, commonly called “liquid foam templating” [11,12], whereas macroporous hydrogels are made by other methods such as ice templating [13,14] or particle leaching [15]. Several reviews already exist on liquid foam [11,12] and emulsion [12,16–19] templating for polymer foams. The present review focuses on hydrogel foams generated from liquid foam templates, the general principle of which is schematised in Figure 1.

In a nutshell, foam templating consists in generating a stable *liquid* foam from a monomer/polymer solution, and subsequently polymerising/cross-linking the continuous phase to obtain a *solid* polymer foam whose structure has been set by the equilibrium of forces in the liquid state and by the solidification procedure. “Solid” refers to the fact that the gel has a finite zero-frequency elastic modulus, i.e. that it cannot flow under applied stresses. The initially wet hydrogel foam can be subsequently dried. This commonly creates a second porosity at the micron-scale which depends on the drying process (see Figure 1 and Section 5.1). Note that we will use throughout this review the term

“solid foam” to describe “wet” hydrogel foams as well as dried hydrogel foams. The main advantage of foam templating is that it exploits the wide knowledge established for liquid foams over the past decades to control the structure of liquid foams [20–23]. Some representative examples of hydrogel foams generated via liquid foam templating and some key properties are given in Figure 2.

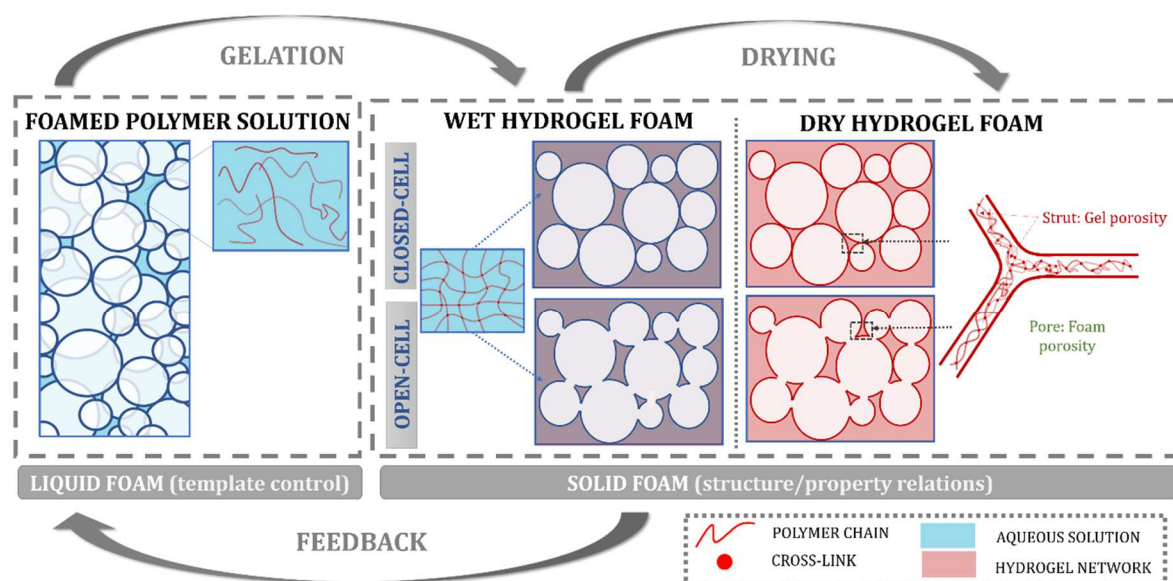


Figure 1: General philosophy of the foam templating route: An initially liquid foam with controlled structural properties is formed from a monomer/polymer solution. Polymerisation/cross-linking of the continuous phase leads to a (wet) hydrogel foam, which is often dried for the final application. The drying generally leads to the creation of a second porosity at the micron-scale. Both, wet and dry hydrogel foams are “solid” in the sense that they cannot flow under applied stresses. Both, wet and dry hydrogel foams can be open- or closed-cell.

Reliable foam templating requires fine control over the structure of the initial liquid foam template, the (physical) chemistry of the foaming liquid and its gelation, as well as over all the involved timescales (foam ageing times, kinetics of polymerisation/cross-linking, or the drying/evaporation time). To obtain a gelled foam having the same morphology as its liquid template, the foam needs to be “frozen” before it destabilises [11]. Yet, solidifying too early may prevent the liquid template to reach its desired structure. An illustrative example is the case of monodisperse foams, which tend to self-order into crystalline structures under the influence of gravity and confinement [24]. This ordering process takes some time and solidifying too early may result in a disordered structure.

This review provides the reader with an overview of the key concepts and parameters to consider when designing a liquid foam template. Section 2 details common ageing mechanisms of liquid foams and how to counteract them to obtain a gelled foam with the desired morphology.

In Section 3 we provide a short summary of some key properties of the hydrogel for the reliable formation of hydrogel foams. We made the choice to concentrate on polymeric hydrogels, excluding superabsorbing hydrogel foams [25–28]. The latter have become particularly popular in recent years due to their impressive absorption capacities. However, their formulation being quite specific, we restricted ourselves here to “classic” hydrogels.

Foam generation is also key to determining its structure, as each foaming method yields a different range of accessible bubble size distributions and liquid fractions [29]. We will thus summarise examples of hydrogel foams produced via different foaming methods, i.e., chemical foaming (Section

4.1) or physical foaming (Section 4.2), to finally summarise some of the key properties of hydrogel foams (Section 5).

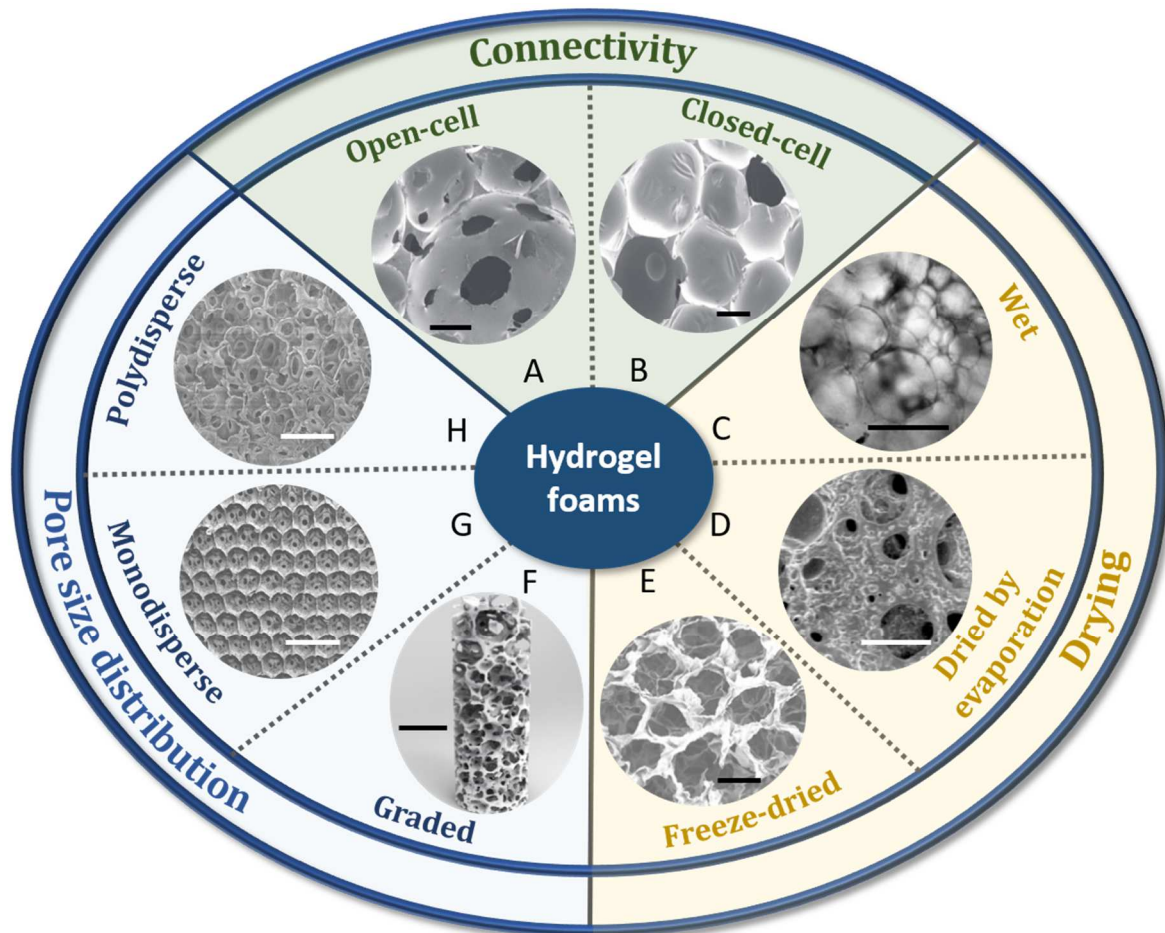


Figure 2: Examples of hydrogel foams generated via liquid foam templating, showing a wide range of accessible structural parameters and states. A and B are polyurethane hydrogel foams, taken from [5]. C is a poly(ethylene glycol diacrylate hydrogel foam), taken from [30]. D is a polyurethane hydrogel foam, taken from [31]. E is a chitosan foam, taken from [32]. F is a computed tomography reconstruction of a gelatin graded foam, taken from [33]. G and H are chitosan foams, taken from [34]. All scale bars are of 500  $\mu\text{m}$  except for graph D where the scale bar is of 50  $\mu\text{m}$ .

## 2. Control over the liquid foam template

### 2.1. Introduction

To obtain hydrogel foams with controlled structural properties, it is essential to control the temporal evolution of the initially liquid foam template. The most important properties of this template are the average bubble diameter  $d$ , its polydispersity, and the volume fraction  $\phi$  of the gas phase. The porosity of the foam is then simply  $100 \times \phi$ . In foam science, one frequently uses the “liquid fraction” for liquid foams, or the “relative density” for solid foams. Both are given by  $(1 - \phi)$ . A wide range of foaming techniques are available for the generation of a liquid foam template with controlled  $d$  and  $\phi$  which are reviewed elsewhere [21,23,29,35]. We discuss here the key mechanisms coming into play once the foam has been generated and how they may be optimised to ensure that the initially liquid foam structure is maintained until the foam is fully gelled. These mechanisms concern how

bubbles pack in foams (Section 2.2), how to avoid that liquid drains between the bubbles (Section 2.3) and that the bubble size evolves with time due to bubble coalescence or gas exchange (Section 2.4), or that foams flow under their own weight (Section 2.5). Tuning these mechanisms involves the tuning of different process-relevant timescales, often in comparison to the characteristic gelation time. We will identify the main physical or physico-chemical parameters here which can be exploited, and we will also show that the overall process optimisation commonly requires to find delicate optima between conflicting tendencies.

## 2.2. Controlling the liquid foam structure

The structure of the foam is controlled by how exactly the bubbles in the liquid template assemble and deform against each other. The key parameters which control foam structure are the gas fraction  $\phi$  and the bubble size distribution, characterised by the average bubble diameter  $d$  and the polydispersity. Their influence is now fairly well understood, and foam scientists can tune between the extremes of low and high density foams, or between monodisperse ordered and polydisperse disordered foams over a wide range of bubble sizes (see Figure 2 for some examples). Several recent books and review articles are available on this subject [20–24,34,36]. We therefore provide here only a very short summary of the most relevant elements.

One speaks about “foams” (in contrast to bubbly liquids or macro-porous materials) when the density of bubbles in the continuous phase is sufficiently high so that all the bubbles touch each other. This is reached above a well-defined gas fraction  $\phi_c$ - the so-called “jamming point” - which corresponds to the situation where all bubbles are spherical and in mechanical contact (close-packed sphere packing). For foams with a moderate polydispersity, this gas fraction can be taken to be  $\phi_c \sim 0.64$ . In monodisperse ordered foams, the bubbles are hexagonally close-packed and one therefore has  $\phi_c \sim 0.74$  [21]. For gas fractions slightly above the jamming point, one speaks of “high-density” foams, while for gas fractions above 0.9 one commonly speaks of “low-density foams”. In liquid foam science, one commonly uses “wet” and “dry” foams, respectively, for these two limits. However, we refrain from using this vocabulary here since it easily creates confusion.

For gas fractions above the jamming point, bubbles deform against each other, creating nearly flat thin films at their contact zones. This creates a three-dimensional assembly of thin films (less than a micrometre thick) bounded by an interconnected network of liquid channels, called “Pleateau borders” in the liquid state and “struts” in the solid state. Close to the jamming point, bubbles in disordered have on average 6 small films, while for gas fractions close to 1, they have on average about 14 films [21]. The characteristic diameter of these films at high gas fractions is of the order of the bubble diameter  $d$ . In between these two extremes, the film size depends not only on the gas fraction, but also on how the bubbles are organised within the foam [37–40]. Since these films are likely to break in a potential pore opening process (see Section 5.3), the gas fraction is an important control parameter to ensure foam stability in the liquid state and to control pore opening in the solid state [39–41].

## 2.3. Maintaining the gas fraction: foam drainage

The most apparent foam destabilisation mechanism is liquid “drainage” which arises in two inter-related manners in a foam: (1) capillary forces drain liquid from the films into the liquid channels, and (2) the liquid in the channel network is driven downwards by gravity. Gravity-driven drainage proceeds until an equilibrium is reached in which gravitational forces are balanced by capillary forces

arising from surface tension. Drainage generally results in an unwanted gradient of gas fraction through the foam. In the worst case, it leads to liquid leaking out of the foam. Both the equilibrium profile of the gas fraction and the drainage dynamics are now well understood [22], providing efficient control strategies to ensure homogeneous liquid foam templates.

The first strategy to maintain a homogeneous template is to gel the continuous phase before drainage has the time to change the liquid distribution measurably. To this end, one can either decrease the gel time or increase the drainage time. The characteristic drainage time can be estimated by [22]

$$\tau_D \sim \frac{\eta}{(1-\varphi)^\alpha d}, \quad (1)$$

with  $\eta$  being the viscosity of the foaming solution,  $d$  the average bubble diameter, and  $\alpha$  (with  $0.5 < \alpha < 1$ ) a dimensionless constant depending on the "mobility" of the liquid-gas interfaces controlled by the stabilising agent. The most efficient way to slow down drainage is, therefore, to work with small bubbles. One can also work with foam stabilisers that make very rigid interfaces ( $\alpha = 1$ ), such as specific proteins; or increase the viscosity of the liquid. One can also optimise the formulation via the polymer concentration or the use of additives to obtain a liquid with shear-thinning properties (the low viscosity under shear facilitates foaming while the higher viscosity in the foam at rest slows down drainage), ideally combined with a finite yield stress which can fully counterbalance gravity in the narrow foam channels and hence stop drainage completely [42–46].

The second strategy is to optimise the equilibrium profile of the gas fraction, i.e., how the gas fraction depends on the height  $h$  in the foam even after longer waiting times. This profile can be approximated by [47]

$$\varphi(h) = 1 - (1 - \varphi_c) \left(1 + \frac{hd}{l_c^2}\right)^{-2}, \quad (2)$$

, where  $l_c = \sqrt{\gamma/\rho g}$  is the capillary length with  $\gamma$  the surface tension of the foaming solution,  $\rho$  its density, and  $g$  the acceleration of gravity.

In order to avoid the most extreme case, i.e., that liquid drains out of a foam of total height  $H$ , one needs to make sure that the gas fraction  $\varphi_0$  of the initially generated foam is larger than the average gas fraction maintained in the foam in equilibrium by capillary forces. Mathematically speaking, one needs to ensure that

$$\varphi_0 > \frac{1}{H} \int_{h=0}^{h=H} \varphi(h) dh. \quad (3)$$

Using a more complete expression (Equation (8) in [47]) than the one given in Equation (2) we numerically calculate Equation(3) using MATLAB for a standard foam with  $l_c^2 = 1.75 \cdot 10^{-3}$  m. This allows us to predict for which  $(d, \varphi)$ -couples the foam will maintain all the liquid even after long waiting times. We obtain the phase diagram shown in Figure 3a for foam heights  $H = 0.5$  cm, 1 cm, 5 cm and 10 cm. All  $(d, \varphi)$ -couples below each curve will maintain all liquid despite drainage. Equation (2) and Figure 3a illustrate the importance to work with small bubbles and a high initial gas fraction, especially if foam heights of several centimetres are sought. For all optimisation with respect to gravity-driven drainage, one needs to keep in mind that the bubble size  $d$  is likely to increase during the foam lifetime due to coalescence and/or coarsening (Section 2.5), making the foam more prone to drainage.

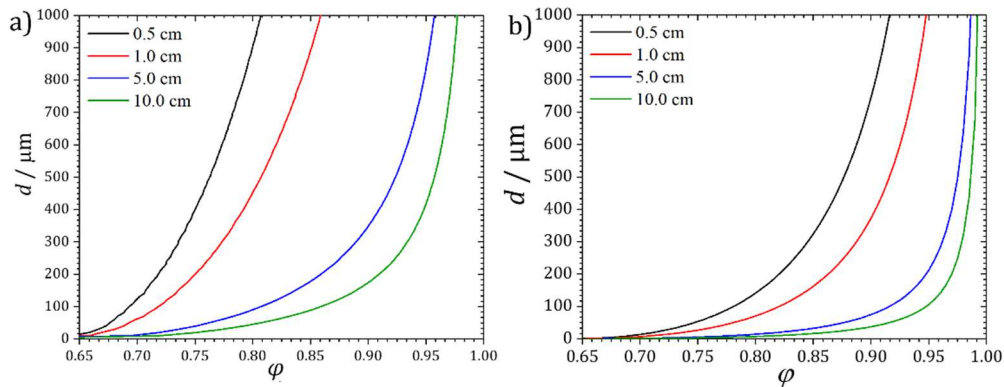


Figure 3: (a) Phase diagram of the average bubble diameter  $d$  and initial gas fraction  $\phi$  for foams of different heights  $H$ . Above each curve, the foams maintain all liquid despite gravity-driven drainage. (b) Phase diagram of the average bubble diameter  $d$  and the gas fraction  $\phi$ , showing curves below which foams of different heights  $H$  remain their shape under the influence of gravity.

#### 2.4. Maintaining foam shape: foam flow under gravity

In many cases, the initial liquid foam template is deposited freely on a surface, as shown in Figure 4. Part of the optimisation process is to make sure that the foam retains its shape under gravity. Due to the presence of closely-packed gas bubbles, liquid foams have the peculiar property of behaving either like an elastic solid or like a viscous fluid depending on the deforming stresses (force per area) they are exposed to. The solid- or fluid-like behaviour of a foam is separated by a well-defined “yield stress” above which the foam starts to flow [21,35,48,49]. This yield stress depends on the foam properties; in particular, it increases strongly with decreasing bubble diameter  $d$  and increasing gas fraction  $\phi$ . An illustrative example of this is displayed in Figure 4, which shows the different flow behaviour of small-bubble foams ( $d \sim 100 \mu\text{m}$ ) under gravity for two different gas fractions  $\phi$ . At  $\phi = 0.85$ , the yield stress is sufficiently low so that the foam flows like a viscous liquid under the gravitational stress, while at  $\phi = 0.95$ , the yield stress is sufficiently high so that the foam behaves like an elastic solid without flowing under the influence of gravity.

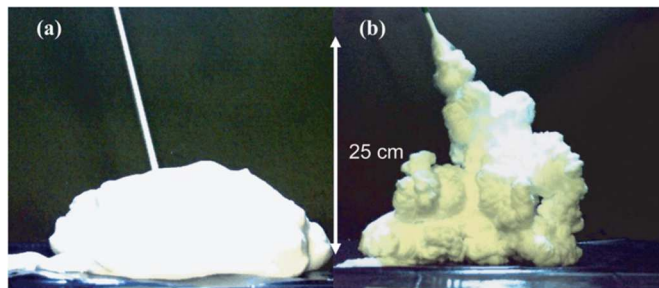


Figure 4: Foams with similar bubble sizes (here ca.  $100 \mu\text{m}$ ) behave very differently under the influence of gravity depending on their gas fraction  $\phi$ . Foams with a low gas fraction  $\phi = 0.85$  (a) flow like a viscous fluid, whereas foams with a high gas fraction  $\phi = 0.95$  (b) behave like a solid, i.e., they retain their shape. Taken from [49].

One can show that the critical height  $H_c$  above which a foam begins to flow under the influence of gravity can be expressed as a function of the bubble size  $d$  and the gas fraction  $\phi$  via [49]

$$H_c = 1.8 \frac{l_c^2 (\varphi - \varphi_c)^2}{d (1 - \varphi)}. \quad (4)$$

Beyond this limit, the gravitational stress overcomes the yield stress of the foam and it flows.

To illustrate the consequences of Equation (4), let us aim to produce a foam of height  $H$ . To avoid that the foam flows under gravitational stress, one needs to ensure that  $H < H_c$ . Equation (4) can then be rewritten to provide a phase diagram of  $(d, \varphi)$ -couples for which this condition is fulfilled. This is shown in Figure 3b for the example for four different foam heights. Below each curve, the foam remains its shape under gravity. Again, one notices the importance of the initial gas fraction and bubble size: larger gas fractions and smaller bubbles allow for higher foam height. One also notices that the criterion of avoiding foam flow puts a stronger constraint on the  $(d, \varphi)$ -couple than the drainage criterion (Section 2.3). Hence, taking care of avoiding foam flow under gravity automatically solves the drainage problem. Finally, foam flow under gravity can also be reduced/avoided by rapid gelation of the foam.

### 2.5. Maintaining the bubble size: coalescence and coarsening

For reliable liquid foam templating, the bubble size needs to be maintained until solidification. Two main mechanisms are involved in increasing bubble size with time: “coalescence” and “coarsening”.

**Coalescence** merges neighbouring bubbles via the rupture of the thin films which separate them. Foam coalescence [50,51] is most easily quantified by monitoring the timeevolution of the foam height and the bubble size distribution. Understanding the main mechanisms leading to bubble coalescence in foams remains an active area of research [52–56]. Nevertheless, vast experimental know-how is already available. Coalescence is mainly dealt with via the formulation to stabilise the thin liquid films, i.e., by choosing the appropriate surface-active agent (often mixtures thereof) at the appropriate concentration [46,52] or by increasing the liquid viscosity to slow down the gravity-driven drainage of the foam (Section 2.3) and the following capillary-driven thinning of the foam films [57].

In **coarsening**, the films remain intact, but gas diffuses between bubbles due to their different pressures and the high permeability of the thin liquid films to gas. Since smaller bubbles have on average larger internal pressures than larger bubbles, they progressively empty themselves into the larger ones until they disappear entirely<sup>1</sup>. After a certain time, which depends on the initial bubble size distribution, the foam reaches a “scaling state” in which only the average bubbles size increases with time. In contrast, the normalised bubble size distribution remains unchanged and of log-normal type [21,35]. In this regime, the bubble diameter  $d$  evolves with time  $t$  as  $d \sim t^{1/3}$  [22]. For foams with a low gas fraction close to  $\varphi_c$  the coarsening dynamics becomes closer to “Oswald ripening” with  $d \sim t^{1/2}$  [58].

To a first approximation, the characteristic time of coarsening is given by [20,21,35]

---

<sup>1</sup> In fact, strictly speaking, the pressure in a foam bubble depends on its number of neighbours [20,21,35], i.e., the number of films. The less neighbours a bubble has, the higher is its pressure. Statistically, smaller bubbles have less neighbours, which is why they are at higher pressures. A foam in which all bubbles have the same number of neighbours would not coarsen. This could be reached with a perfectly periodic foam. However, experimentally this is impossible to reach. The presences of a few defects is sufficient to start coarsening around the defect. However, in comparison to polydisperse foams, the coarsening process is slowed down.

$$\tau_{\text{coars}} \sim \frac{d^2}{D_{\text{eff}} F(\varphi) \kappa}, \quad (5)$$

where  $D_{\text{eff}}$  is an effective diffusion coefficient which depends on the solubility of the gas, its diffusion coefficient in water, and the permeability of the surfactant layer to the gas.  $\kappa$  is the film thickness and  $F(\varphi)$  is the fraction of the bubble surfaces covered by thin films (the higher the gas fraction, the larger  $F(\varphi)$  – see Section 2.2). Equation (5) evidences again the importance of the gas fraction  $\varphi$  and the bubble size  $d$ . In contrast to drainage and foam flow, however, small bubbles are a disadvantage here since they greatly accelerate coarsening through the  $d^2$ -dependence.

Coarsening is thus a complex phenomenon that depends on an interplay of structural and physico-chemical parameters of the foams. This interplay provides different levers to slow down coarsening. These levers rely on (i) the bubble size distribution, (ii) the solubility of the gas and related osmotic effects, (iii) the rheological properties of the gas-liquid interface (interfacial elasticity), and (iv) the elasticity of the bulk phase.

- (i) Since the driving force of coarsening is the pressure difference between bubbles, the initial degree of polydispersity and order can be used to control the time until the foam enters the scaling state. The more monodisperse and ordered a foam is [20,21,24,35], the slower its coarsening dynamics. This is why the use of highly monodisperse foams generated by microfluidics has become popular in academic research, although it is less practical for industrial applications [59–61].
- (ii) A commonly used method to slow down coarsening is to work with gases of *low solubility*, which decreases  $D_{\text{eff}}$  in Equation (5). For example, a foam prepared using  $\text{N}_2$  will coarsen much more slowly than a  $\text{CO}_2$ -based foam due to the lower solubility of  $\text{N}_2$  in water [21]. A more pronounced effect is obtained by adding traces of water-insoluble *gas/vapour* molecules to the bubbles [62,63]. Commonly, perfluorocarbons such as perfluorohexane  $\text{C}_6\text{F}_{14}$  are used. Being insoluble in water, these molecules cannot transfer between bubbles to re-equilibrate their chemical potential, which is modified by the volume changes of bubbles upon coarsening. As such, an osmotic pressure difference is created between neighbouring bubbles, which counteracts the Laplace pressure and stops coarsening. If the initial concentration of the insoluble gas is too low, the foam will undergo coarsening until the osmotic pressure differences are high enough [62,64], commonly leading to the presence of large bubbles. However, a critical concentration  $C_c$  of insoluble species above which the generated foam will be immediately stable against coarsening can be identified [62,64]. Assuming one larger or smaller bubble in a hypothetical monodisperse foam with bubble diameter  $d$  in which all bubbles have the same pressure, Bey et al. [64] predict and experimentally confirm that this critical concentration  $C_c$  (number of molecules per unit volume) can be estimated as

$$C_c = \frac{2 \gamma f(\varphi)}{3 d k_B T}, \quad (6)$$

where  $k_B$  is the Boltzmann constant,  $T$  the temperature and  $f(\varphi)$  a function of the gas fraction related to the capillary pressure of the bubbles. If the added component is not completely insoluble, coarsening proceeds nevertheless, but over much larger timescales given the much smaller  $D_{\text{eff}}$  of the poorly soluble gas (Equation (5)).

However, a side effect of using an insoluble gas species may be the significant swelling of foams in contact with an atmosphere not containing the same insoluble gas species. In

this case, the difference of chemical potential with the atmosphere leads to an efficient migration of air into the bubbles to dilute the concentration of insoluble species [65]. This phenomenon may be stopped by keeping the foams in the same gas mixture as the one contained in the bubbles or by shielding the foams from the atmosphere.

- (iii) Another highly efficient approach to hinder coarsening exploits interfacial elasticity arising from stabilising agents [66–69]. Many polymers, particles, lipids or proteins may be irreversibly adsorbed to the bubble surface. Coarsening modifies the surface area  $A$  of the bubbles resulting from their volume change. This modification of the surface area leads to a change in the surface concentration of the stabilising agent, modifying the surface tension  $\gamma$ . How much surface tension changes upon dilation/compression is commonly expressed by the Gibbs dilational elastic modulus [70]

$$E_d = \frac{d\gamma}{d\ln(A)}. \quad (7)$$

Integration of Equation (7) leads to the description of the surface tension with surface dilation  $A/A_0$  away from the reference state  $A_0$  at  $\gamma_0$ :

$$\gamma(A) = \gamma_0 + 2E_d \ln\left(\frac{A}{A_0}\right). \quad (8)$$

This shows that upon bubble growth, the effective tension is increased by elasticity, while upon bubble shrinkage, the effective tension decreases down to  $\gamma(A=A_c) = 0$ , giving

$$A_c = A_0 \exp\left(-\frac{\gamma}{2E_d}\right). \quad (9)$$

Since the bubble pressure  $P$  is proportional to the surface tension, it becomes zero at this point and the driving force for coarsening stops. For this situation to be physically stable, one also needs the condition that  $dP/dA > 0$  [66–69,71]. I.e., if the bubble grows ( $dA > 0$ ), its pressure increases ( $dP > 0$ ), promoting bubble shrinkage, while if it shrinks ( $dA < 0$ ), the pressure becomes negative ( $dP < 0$ ), sucking in gas from the environment to make the bubble grow again. For an isolated bubble, this leads to the Gibbs criterion, which fixes the ratio of elastic modulus and surface tension above which gas diffusion from the bubble stops [71]:

$$\frac{E_d}{\gamma} > \frac{1}{2}. \quad (10)$$

This ratio may be considered as a non-dimensional elasto-capillary number. While the Gibbs criterion can be rigorously derived for individual bubbles, the complex response of polydisperse foams requires more careful consideration [72]. However, the general idea remains valid.

The Gibbs dilational elastic modulus can be experimentally measured via bubble/drop shape tensiometry or using a Langmuir trough [73]. Formulation can help reach this interfacial elasticity criterion by choosing the adequate surface-active agent (or a mixture thereof) [66–69]. Note that high interfacial dilational elasticities can also be achieved by creating a solid interface, e.g., through physical or chemical cross-linking of the interface. Highly elastic interfaces are often also dense, reducing gas diffusion through the thin films and hence coarsening (see point ii).

- (iv) So far, all the means of hindering coarsening have been defined for liquid foams. However, we are interested in this review in foams that can gel, i.e., whose continuous phase can become elastic with an elastic shear modulus  $G$ . Beyond a critical elastic shear

modulus  $G_c$ , the elastic response of the foam can balance the capillary stresses driving coarsening. For a foam with average bubble diameter  $d$ , one can estimate the elastic energy as  $G \sim F(\varphi)d^3$ , where  $F(\varphi)$  is again a function that takes into account the gas fraction. The surface energy, which is the driving force for coarsening, can be estimated by  $\gamma d^2$ . Coarsening stops when both energies are of the same order of magnitude, giving

$$\frac{G_c}{\gamma} \sim \frac{F(\varphi)}{d}. \quad (11)$$

As in Equation (10), this shows the importance of the ratio of the elastic modulus (here shear modulus  $G$ ) to the surface tension  $\gamma$ . However, since the elastic force is here a bulk force, the bubble diameter  $d$  becomes an important control parameter in fixing the critical shear modulus  $G_c$  of the gel to stop coarsening. I.e., the smaller the bubbles, the stronger the gel needs to be. More detailed relationships can be obtained for individual bubbles [71] or foams [64].

One can combine the different mechanisms (i)-(iv) to efficiently stop coarsening. While investigations on individual bubbles are advanced, systematic investigation and modelling of the coupling of these different effects in foams are still lacking. For example, Bey et al. [64] investigated the combination of a gelling matrix and an insoluble gas species. They produced stability phase diagrams showing for which ranges of bubble sizes and concentration of insoluble gas the foams are stable against coarsening.

In general terms, it is essential to note that the gas fraction  $\varphi$  is a key control parameter for coalescence and coarsening, always in a manner that an increasing gas fraction leads to more pronounced coalescence or coarsening. Since foam drainage (Section 2.3) modifies the gas fraction, it must be considered together with coalescence and coarsening.

### 3. Control over the continuous hydrogel phase

This section focuses on the characterisation and control of the properties of the continuous phase, i.e., of the hydrogel network. Hydrogels are viscoelastic polymer matrices consisting of a three-dimensional cross-linked network of hydrophilic homopolymers, copolymers, or macromers swollen in water. Hydrogels are able to take in a large amount of water without dissolving [74]. The solid content in a hydrogel (i.e., polymer and cross-linker) is very low compared to the water content [75] and it can be as low as 1 wt.% [76]. This dilute nature allows for the passive diffusion of solutes within hydrogels. While designing hydrogel materials, one commonly aims for the following properties (depending on the application): biocompatibility and biodegradability, maximum equilibrium swelling capability in saline, high absorbency under load (AUL), low residual monomer and soluble content, high stability, maintenance of pH-neutrality after swelling in water or photostability [8].

In this Section, we discuss the key elements for optimising the continuous phase of hydrogel foams. We discuss the cross-linking mechanisms (Section 3.2) and the kinetics of gelation (Section 3.3).

#### 3.1. Classification of hydrogels

Polymeric hydrogels are commonly scatergorised according to different parameters. In terms of the origin of the polymers, they may be classified into *synthetic hydrogels* (e.g., poly(ethylene glycol), polyvinyl alcohol, polyphosphazene) [77,78] or *natural hydrogels*. Natural polymers are either *animal-derived* (e.g., collagen, fibrin, chitosan, hyaluronic acid, silk) or *plant-derived* (e.g., alginate, pectin, xanthan, carrageenan). Natural polymers have large molecular sizes (can vary from  $10^4$  to  $10^6$  g/mol for commercial chitosan, for example) and are readily available [78,79]. Synthetic and natural polymers can also be combined in hybrid hydrogels. For example, Wang et al. [80] combined a protein and N-(2-hydroxypropyl)-methacrylamide for enhanced delivery properties.

It is also commonplace to distinguish *physical hydrogels* from *chemical hydrogels* according to the nature of the cross-links (Section 3.2). Hydrogels can also be classified based on their sensitivity to stimuli [78,81], porosity [82,83], polymer configuration (nanocrystalline, semicrystalline, crystalline), physical appearance (micro, nano, particle, matrix, film, etc. ), the charge of the polymeric network (ionic, nonionic, amphoteric, etc.), or the composition of the polymer (homopolymer or copolymer) [84,85].

#### 3.2. Nature of cross-links

Multiple approaches are used to create physical and chemical hydrogels. The most common ones are summarised in Table 1. **Chemical cross-links** are irreversible covalent bonds that can be formed via two methods: (1) cross-linking during polymerisation of monomers (condensation polymerisation, free radical polymerisation, or plasma polymerisation) or (2) cross-linking of existing polymer chains. **Physical cross-links** are obtained by reversible physical interactions between polymer chains. These include ionic interactions, hydrophobic interactions, crystallisation, hydrogen bonding or entanglements. These interactions can be controlled by a wide range of parameters, including pH, ionic strength or temperature variations (e.g., cryogenic treatment).

Ionic cross-linking is commonly achieved by the addition of other molecules such as multivalent ions of opposite charge to the polymer [86–88] or by the aggregation of oppositely charged polymers. Cross-linking of amphiphilic or grafted polymers that contain hydrophobic blocks can take place via hydrophobic interactions when decreasing the overall solubility of the molecules by means of external stimuli (temperature, pH, ionic strength). The gelation temperature depends on the

concentration of the polymer and the polymer structure [89]. One of the common polymers that undergo reverse thermal gelation are triblock copolymers of poly(ethylene oxide)-poly(propylene oxide)-poly(ethylene oxide) (PEO-PPO-PEO), where the gelation temperature is close to physiological temperature [90].

Hydrogen bonding interactions are considered as physical cross-links but are often accompanied by the formation of other types of interactions, for example, peptide and ester bonds [91]. In the case of injectable hydrogels and unless no other form of cross-linking is used for the gelation, these hydrogels are limited to short-acting drug release as the network is diluted and dispersed in vivo due to water influx.

Semi-crystalline hydrophilic polymers are classified as hydrogels considering that the crystallites act like physical cross-links and are insoluble in water [92]. Physical entanglements are also considered as cross-links and form weak hydrogels [93].

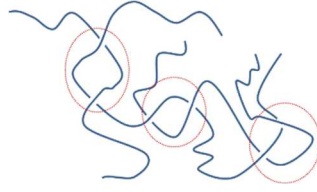
Table 1: Most common cross-linking routes for hydrogel preparation.

	Cross-linking method	Cross-linker	Mechanism	Examples
Chemical cross-links	Cross-linking while polymerising monomers	Co-monomer with functionality > 2 External cross-linker		[94–96]
	Cross-linking of homopolymers	External bifunctional or multifunctional cross-linker		Functionality = 2 [97–99] Functionality >2 [100,101] Photo-cross-linking [102,103]
Physical cross-links	Cross-linking by ionic interaction	Polyelectrolytes Divalent ions		[86–88,104–106]
	Cross-linking by hydrophobic interaction	∅		[90]
	Crystallisation	∅		[107]
	Cross-linking by hydrogen bonding	∅		[91,108,109]

---

Entanglements

$\emptyset$



[93]

### 3.3. Kinetics of gelation

A hydrogel is formed by the progressive formation of a cross-linked network, which turns a viscoelastic liquid (the “sol”) into a viscoelastic solid (the “gel”). During this gelation process, the system passes through a well-defined “gel point” [110] at a well-defined “gel time  $\tau_G$ ”, at which the viscosity of the system diverges, and the solid-like elasticity steeply increases. Controlling the kinetics of gelation is crucial in liquid foam templating since the gel point has to be matched to the characteristic timescales of the different foam processes (Section 2). Successful liquid foam templating, therefore, requires a careful choice of the appropriate gelling formulation for a given foaming process and the final application.

The gelation kinetics and associated gel time can be measured using different methods [111,112]. The most common method is to use shear rheology to follow the evolution of the elastic and viscous shear moduli,  $G'$  and  $G''$ , respectively, as a function of time, as shown in Figure 5a. Historically, as suggested by Tung and Dynes [113] in 1982, the gel time was taken as the time of the crossover point of the two moduli, i.e.,  $G' = G''$ . However, it was quickly realised that for many gels this point depends on the shear frequency  $\omega$ . More specifically, Winter [114] showed that at the gel point, both,  $G'$  and  $G''$  show a power-law behaviour (Figure 6c) with

$$G' = \frac{G''}{\tan(n\pi/2)} \sim \omega^n, \quad (12)$$

with  $0 < n < 1$ . Hence, at the gel point, the phase angle is constant and given by

$$\tan \delta = \frac{G'}{G''} = \tan(n\pi/2). \quad (13)$$

A schematic illustration of the viscoelastic response of a hydrogel undergoing gelation is shown in Figure 5. This universal scaling defines the gel point and has now been confirmed for a wide range of systems [115]. It has also led to the elegant “multi-wave” method, which is starting to be implemented on most rheometers. In this method, as shown in Figure 5b, the gel point is taken as the point where measurements of the ratio  $G''/G'$  at different frequencies coincide. This point coincides with  $G'=G''$  only if  $n = 1/2$ , which has been shown to hold for few systems only. In most cases  $n > 1/2$ , which is commonly associated with imbalanced stoichiometry or other network imperfections [114–116]. Great attention should be given to the working temperature since the sol-gel transition is temperature-dependent, and the strength of the network at the gel point decreases with temperature [117].

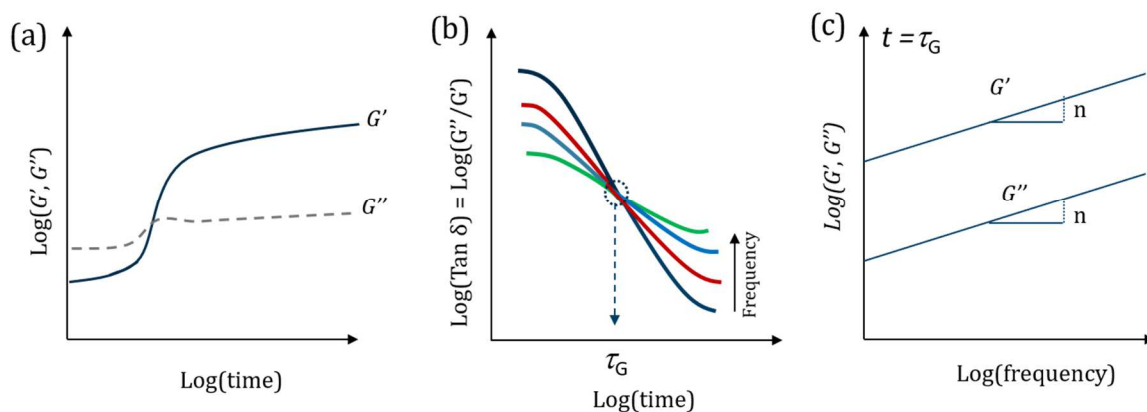


Figure 5: Characteristic evolution of the elastic shear and viscous shear moduli,  $G'$  and  $G''$  during gelation. (b) Illustration of the variation of  $\tan \delta$  with time during hydrogels gelation. (c) Illustration of frequency sweep at the gel point determined from (b). Redrawn from [41,112,118].

Fine-tuning the formulation provides control over the kinetics of gelation [119]. For example, the gel time is reduced with increasing cross-linking initiator concentration [120] and with increasing polymer concentration [118]. In the case of physical gelation by means of divalent ions, gelation kinetics is controlled by varying the concentration of ions [121], the nature of ions and/or ion ratio for ion mixtures [122].

## 4. Hydrogel foams from liquid foam templates

We report in this Section different existing systems of hydrogel foams. We chose to divide them according to the used foaming process to gain insight into its effect on the final hydrogel foam properties and their potential applications.

We recommend reading [29] for more information about the foaming techniques available and the physics behind them. Here, we distinguish two main categories, namely, chemical foaming (Section 4.1) and physical foaming (Section 4.2). For physical foaming, we distinguish between mechanical foaming (Section 4.2.1), and foaming by gas injection, with a focus on microfluidic foaming (Section 4.2.2).

### 4.1. Chemical foaming

Chemical foaming uses the in-situ release of gas via chemical reactions. The foaming agent inducing gas generation can be either a co-product of the cross-linking reaction or external.

Table 2 presents examples of chemically foamed hydrogels along with additional information on the hydrogel (polymer, cross-linker), foaming reaction, and foam properties (bubble size, pore connectivity, porosity). Characteristic pore sizes are of the order of 50-1000 micrometres with a large range of porosities. Note that most of the hydrogel foams are polydisperse with open cells.

The only examples where the chemical gelation reaction produces the gas in situ are polyurethane hydrogel foams. In preparing polyurethane foams, isocyanate reacts with water( or other agents like boric acid [123]) forming gaseous carbon dioxide and an amine which reacts with another isocyanate forming a urea bond. Surfactants are used to stabilise the generated bubbles and avoid the dissolution of CO<sub>2</sub> in the liquid. Note that not all polyurethane foams can be qualified as hydrogels, but, in the examples we cite here, the polyols were dissolved in water [5,31,124]. These materials were used for tissue engineering and wound healing thanks to the biocompatibility of polyurethane. A challenging problem remains that CO<sub>2</sub> is highly soluble in water, favouring foam coarsening (Section 3.1). David et al. [31] proposed that by enhancing the rate of polymerisation, one may reduce the bubble size to fit the application.

Using intrinsic foaming does not only limit the chemistry and the choice of the blowing gas, but also other formulation parameters. For instance, Lundin et al. [5] observed that the pore size increases with decreasing cross-linking density. The presence of a non-ionic surfactant resulted in a reduction of the average pore sizes of about 35%.

As one can see in Figure 6, polyurethane foams with different formulations yield different morphologies. Figure 6a shows a PU hydrogel foam with closed-cell structure. Changing the poly(ethylene glycol):glycerol ethoxylate mole ratio, PEG molecular weight, and adding a non-ionic surfactant resulted in the formation of an open-cell structure (Figure 6b) with larger pores. What remains unknown is which of these three parameters controls the pore opening. The authors argue that the presence of surfactant induces an open-cell structure but proposed no mechanism to explain this behaviour.

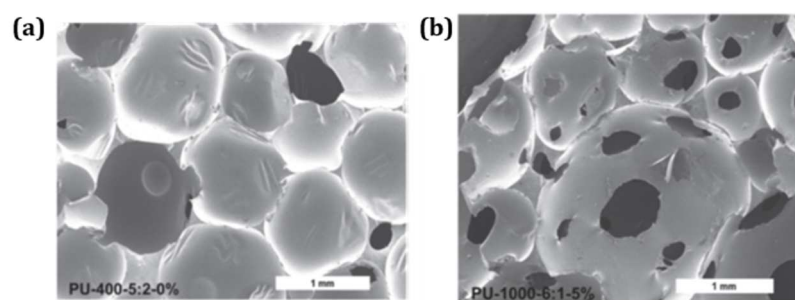
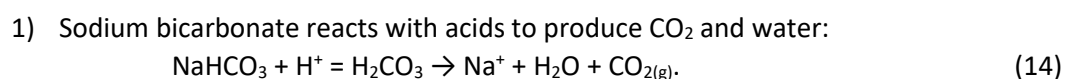


Figure 6: SEM micrographs of two polyurethane hydrogel foams with different compositions. (a): Poly(ethylene glycol) molecular weight= 400, poly(ethylene glycol):glycerol ethoxylate mole ratio= 5:2, stabilizer concentration = 0 wt.%. (b): Poly(ethylene glycol) molecular weight= 1000, poly(ethylene glycol):glycerol ethoxylate mole ratio= 6:1, stabilizer concentration = 5 wt.%. [5]

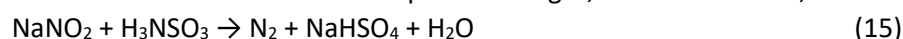
In addition to external chemical agents, the addition of a foaming aid (e.g., an acid triggering the blowing reaction) and a foam stabiliser to the polymer solution is often necessary. We identified from the literature three foaming reactions:



Sodium bicarbonate being a basic component, it neutralizes the acid. Researchers used this foaming route to foam PEG- [30,120,125], gelatin- [126], alginate- [122,127,128], chitosan- [129], and acrylic acid- [26,130,131] based hydrogels.

In the case of acrylic acid being the monomer, no additional foaming aid is required, as the acid groups of the monomer react with sodium bicarbonate to generate CO<sub>2</sub>. This can be a limitation in terms of control over the kinetics of foaming and gelation, as here, the gelation reaction starts immediately after the sodium bicarbonate is added, which is not the case when the acid is added at a later stage. Another case where the acid is part of the gelation system is when a redox pair initiate the polymerisation. However, in this case, the pH variation will significantly affect the gelation kinetics. For example, in the case of ammonium persulfate/ascorbic acid (APS/AH) initiation system, the decrease of pH results in a decrease of the production of free radicals. When producing microporous poly(propylene fumarate-co-ethylene glycol) hydrogels, the gelation was completely inhibited for a formulation with twice the molar concentration of AH compared to APS [120]. This is a complex problem since acidic pH is required for the foaming reaction. pH adjustment of the monomer solution is then required in order to control the foaming and gelation times [25].

- 2) Sodium nitrite reacts with sulfamic acid to produce N<sub>2</sub> gas, sodium bisulfate, and water:



An advantage of this route is that N<sub>2</sub>-based foams coarsen much less than CO<sub>2</sub>-based foams (Section 3.1). Barbetta et al. [132] used this method to successfully prepare gelatin-based foams with an average pore size of 230 μm. Even though this is the only example we found, this method should be readily applicable to other hydrogels.

- 3) Another chemical foaming method was introduced by Tang et al. [133], who used the hydrolysis of magnesium particles as a hydrogen-producing foaming method



Although the material was not a foam-templated hydrogel (foaming occurred simultaneously to gelation), this method could be used in a foam templating route. For example, one could use the Mg<sup>2+</sup> ions generated during the foaming reaction to generate ionically cross-linked hydrogels (e.g. alginate, see Section 3.2 ). As reported in [134], magnesium ions can cross-link sodium alginates in a slow gelation process (2-3 hours), ensuring that gelation occurs after foaming.

As cited above, most studies have relied on inorganic blowing agents. However, many organic foaming agents exist, including Azodicarbonamide (ADCA), barium azodicarboxylate, Oxybis(benzenesulphonyl hydrazide (OBSH), p-Toluenesulphonyl hydrazide (TSH), N,N'-dinitrosopentamethylenetetramine or Toluenesulphonyl semicarbazide (TSS) [135,136]. As far as we are aware, their use remains to be explored for the formulation of hydrogel foams.

Table 2: Examples of different hydrogel foams generated by chemical foaming. All foams are polydisperse. EDC is 1-ethyl-3,3-[3-(dimethylamino)propyl] carbodiimide hydrochloride, and NHS is *N*-hydroxysuccinimide.

Ref	Hydrogel type	Polymer	Cross-linker	Foaming reaction	Range of pore diameter $d$ / $\mu\text{m}$	Open-/closed-cell	Porosity / %
[5]	Chemical	Polyurethane	Diisocyanate	Diisocyanate with water	600-1200	Closed to Open	
[31]	Chemical	Polyurethane	Diisocyanate	Diisocyanate with water			
[124]	Chemical	Polyurethane	Diisocyanate	Diisocyanate with water	~ 100	Open	~ 80
[125]	Chemical	Polyethylene glycol (PEG)	Diacrylate	Sodium Bicarbonate with acrylic acid	~20-80	Open	~ 57-67
[30]	Chemical	Polyethylene glycol (PEG)	Diacrylate	sodium Bicarbonate with acid	100-600		
[120]	Chemical	Poly(propylene fumarate-co-ethylene glycol)	Poly(ethylene glycol) diacrylate	Sodium bicarbonate with acid	50-200	Open	66- 84
[126]	Chemical	Gelatin	Glutaraldehyde	Sodium carbonate with acetic acid	280-550	Open	
[132]	Chemical	Gelatin	EDC	Sodium nitrile with sulfamic acid	~ 230	Open	
[127]	Chemical	Alginate	EDC/NHS	Sodium bicarbonate	180-260	Open	
[128]	Physical	Alginate	Metal salt	Effervescent compound with acid	NA		
[122]	Physical	Alginate	Strontium carbonate/calcium carbonate	Sodium bicarbonate with d-glucono- $\delta$ -lactone	100-400	Open	35-50
[129]	Chemical	Chitosan	Glyoxal	Sodium bicarbonate with acid	NA		
[26]	Chemical	Poly(acrylic acid)	<i>N,N</i> -methylene bisacrylamide	Sodium bicarbonate with acrylic acid + acetone as porogen	NA	Open and closed	
[130]	Chemical	Poly (acrylic acid) (PAA)	Inner cross-linker	Sodium bicarbonate	NA	Open	

				acrylic acid			
[131]	Chemical	Poly(acrylic acid) Poly(acrylamide)	N,N'-methylene bisacrylamide	Sodium bicarbonate	NA	Open	69-84

## 4.2. Physical foaming

### 4.2.1. Mechanical foaming

Another commonly used processing technique for generating foam-templated hydrogels is mechanical foaming. One way to mechanically generate bubbles is gas entrainment at freely-flowing surfaces followed by bubble break-up under shear [29]. The most classic example is the kitchen blender or Ultra-Turrax, as schematically sketched in Figure 7a. The process leads to a progressive increase of the gas fraction and a decrease of the average bubble size over time until an equilibrium is reached. Gas fraction and bubble size at equilibrium depend on the rheological properties of the foaming liquid, on the power input and on the geometry of the rotating element. Typically, a two-steps process is used to produce mechanically foamed hydrogels [137–140]. The first step consists in producing the liquid foam which is followed by initiation of the gelation reaction either by adding the cross-linker or catalyst under continuous shearing or by thermal treatment. Table 3 presents examples of different hydrogel foams obtained by mechanical foaming. These materials are polydisperse with average pore sizes ranging from 50 to 500  $\mu\text{m}$ .

Hsieh et al. [141] controlled the pore size of chitosan hydrogel foams by tuning the mechanical energy input. They demonstrated that faster stirring rates produced foams with smaller pore diameters (from 500  $\mu\text{m}$  at 2000 rpm to about 400  $\mu\text{m}$  at 4000 rpm) until reaching a critical speed (4000 rpm) above which the change in pore size was minimal. The authors also showed that increasing the stirring rate or the chitosan concentration lowered water absorption capacity.

Using mechanical stirring the gas phase to atmospheric air. One technique that offers the choice of the gas phase is the double syringe technique [142] (sketched in Figure 7b) which consists of mixing the foaming liquid with the selected gas by repeatedly passing both through tubing from one syringe to another. This technique also has the advantage to provide reproducible bubble size at a controlled liquid fraction as it allows setting both the liquid and the gas volume within the foam. Zowada et al. [143] used this technique to produce AMPS-based hydrogel foams with an average pore size of 63  $\mu\text{m}$  at 70% porosity. Using this simple technique, one can vary the liquid fraction without affecting the bubble size distribution. Moreover, it gives the possibility of producing foams with high porosities and small bubble sizes required for many applications. It is mainly used in healthcare applications [142].

Choice of gas and addition of gelation trigger can be controlled in the case of the mechanical stirring route when working in a closed system with gas and liquid loading tubes, as shown in Figure 7c. The double-syringe technique can be adapted in a similar spirit by adding a third syringe to add the gelation trigger to a pre-foam at a given moment (Figure 7d).

The gelation kinetics of the system should be considered when foaming the solution. In fact, vigorous stirring after gel formation can “break” the cross-links formed in an irreversible way, negatively affecting the elasticity the gel or leading to foam collapse. For example, PVA foams cross-linked with borax demonstrated a shear-induced coalescence of the foam when low polymer/cross-linker ratios were used. However, stable foams were obtained for high polymer/cross-linker ratios [138]. This shear-induced coalescence was observed below a critical ratio of entanglements/borax ions per chain. It is therefore important to have a clear idea of the gelation time (see Section 3.3) to ensure that the gel point occurs after foaming. Note that there might be confinement effects within the foam that may alter the gelation kinetics compared to bulk gelation. Much insight is still required on how foaming may affect gelation.

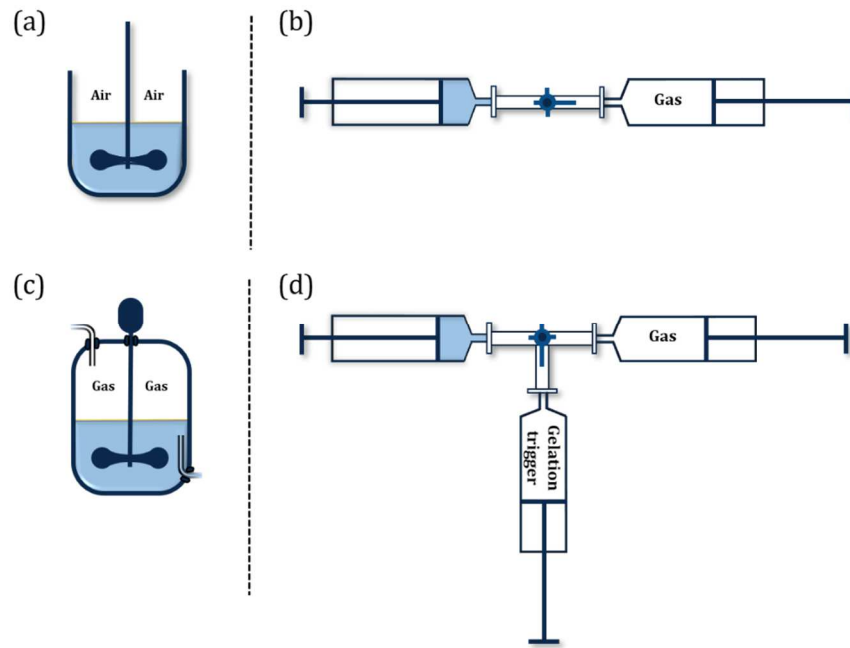


Figure 7: Schematic illustrations of two commonly mechanical foaming techniques: (a) Mechanical stirring of the foaming liquid (blue). (b) Double-syringe technique where two syringes are connected, one containing the gas, the other containing the foaming liquid. Below, suggestions for modified foaming processes: (c) Mechanical stirring in a closed system where the gas can be different from ambient air, and liquids can be added during foaming. (d) Modified double-syringe set-up in which the gelation trigger can be introduced after the formation of a pre-foam.

Table 3: Examples of different hydrogel foams generated by mechanical foaming. Mechanical foaming was ensured by vigorous stirring at high speed.

Ref	Hydrogel type	Polymer	Cross-linker	Foaming technique	Pore diameter $d$ / $\mu\text{m}$	Open-/ closed-cell	Porosity / %
[137,138]	Physical	PVA	Borax	Beater mixer	400		
[144]	Chemical	PVA / chitosan	Tetraethoxysilane	High shear mixer	500		
[141]	Physical	Chitosan	Self-cross-link	High shear mixer	200 - 500		> 80
[145]	Chemical	Chitosan/Gelatin	Tannic acid	High shear mixer		Open	
[146]	Physical	Alginate	Calcium ions	High shear mixer	100-200	Open	80-98
[139]	Physical	Alginate	Calcium carbonate	Beater mixer	< 500	Open	
[147]	Physical	Alginate	Calcium carbonate	Beater mixer		Open	
[148]	Physical	Propylene glycol alginate: PGA	Calcium carbonate	Balloon whisk			40 - 60

[140]	Chemical	Polyacrylamide	N,N'-methylenebisacrylamide	Vertex mixer	50 - 130	from open to close	73 - 81
-------	----------	----------------	-----------------------------	--------------	----------	--------------------	---------

#### 4.2.2. Foaming by gas injection

Gas injection is a very intuitive mechanical foaming method, as children do it when blowing into a straw to make large bubbles in their drinks. Injecting gas into a liquid which can be gelled constitutes an efficient foam templating route. We distinguish here two types of gas blowing: (1) batch foaming, in which the gas is injected from below into the foaming liquid that is either static or stirred (Section 4.2.2.1); and (2) microfluidic foaming (Section 4.2.2.2). Examples from the literature are gathered in Table 4 together with some key parameters.

##### 4.2.2.1. Batch foaming

Batch foaming has been used to produce polysaccharide-based hydrogel foams [149–152] or poly(vinyl alcohol) foams cross-linked with glutaraldehyde [153]. An example of a gas injection set-up is shown in Figure 8. The foaming liquid is placed in a thermostated reactor allowing for foaming at elevated temperatures, which is mandatory for some systems such as gelatin, which physically gels at room temperature [149]. The gas is injected at a constant flow rate with the help of a syringe pump. Ensuring a constant gas flow rate during the injection process is necessary to ensure control over the bubble size [29]. However, the main parameter controlling the bubble size is the diameter of the pores in the porous glass septum. For low gas flow rates (quasi-static regime), the bubble size varies proportionally with the pore size [29].

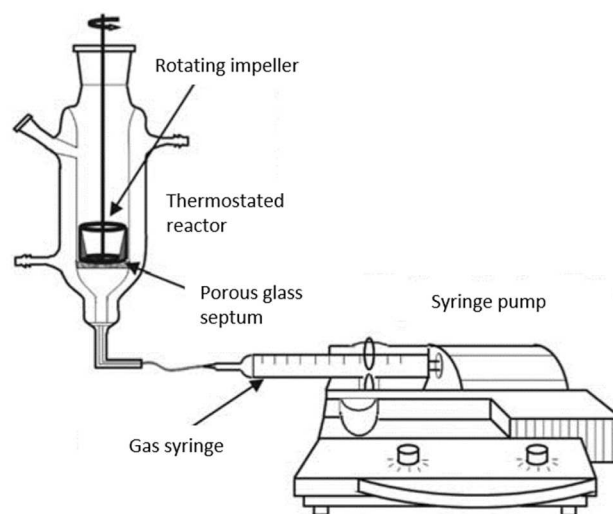


Figure 8: Common gas injection set-up for the batch generation of hydrogel foams. Adapted from [149].

The set-up displayed in Figure 8 is more complex since the reactor contains a rotating impeller keeping the foam homogeneous during foaming [149]. Stirring the foam allows to delay drainage (Section 2.3) until the foam is fully generated. Moreover, although we found no example of it in the literature, one may imagine that for large bubbles and high rotating speeds, the impeller could be used to break bubbles down and decrease the average bubble size in the foam (Section 4.2.1).

A pressure controller can be used for gas injection instead of a syringe pump. However, the syringe pump presents several advantages such as a steady flow rate and a precise control of the injected volume, allowing to set the liquid fraction of the foam.

To avoid foam ageing issues until the foam is gelled (Section 2), a possible protocol is to withdraw the foam from the reactor as soon as gas injection is finished and freeze it with liquid nitrogen. Once frozen, the foam is no longer subject to destabilisation and can be freeze-dried. However, such a foam is, although solid, not cross-linked. Cross-linking can be carried out by subsequently soaking the freeze-dried foam in a solution containing the cross-linker. Although a clever workaround to foam stability issues, the multi-step and batch nature of this process is heavy and freeze-drying limits the volume of the foams which can be generated.

The foams generated with this method have rather small pore sizes, the largest being 500  $\mu\text{m}$  (see Table 4). However, one could expand the range of pore sizes available with this foaming technique by tuning the pore size of the porous glass septum, larger pores yielding larger bubbles.

Table 4: Examples of different foam-templated microporous hydrogels generated by gas injection, with the distinction between batch and microfluidic foaming.

Ref	Hydrogel type	Polymer	Cross-linker	Pore diameter $d$ / $\mu\text{m}$	Open-/closed-cell	Porosity / %
<b>BATCH FOAMING</b>						
[153]	Chemical	Poly(vinyl alcohol)	Glutaraldehyde	210 $\pm$ 95	Open	78
[149]	Chemical	Gelatin	EDC	250-360	Open	86-89
[152]	Chemical	Gelatin	EDC	250 $\pm$ 20	Open	83
[150]	Chemical	Hyaluronic acid	EDC	100-350	Open	87
[150]	Chemical	Chitosan	Genipin	100-500	Open	92
[150]	Chemical	Alginate	EDC	100-350	Open	85
[151]	Physical + Chemical	Alginate	Calcium ions EDC/NHS	20-280	Open	66
<b>MICROFLUIDIC FOAMING</b>						
[32]	Chemical	Chitosan	Genipin	338 $\pm$ 8 644 $\pm$ 30	Open	
[34]	Chemical	Chitosan	Genipin	364 $\pm$ 14 322 $\pm$ 48	Open	99 99
[154]	Chemical	Chitosan	Genipin	$\sim$ 300	Open and Closed	99
[155]	Physical	Alginate	Calcium ions	50-180	Open	
[156]	Physical	Alginate	Calcium ions	$\sim$ 200 <sup>2</sup>	Open	87
[157]	Chemical	Methacryloyl gelatin	Self cross-linking	240-360	Open and Closed	
[39]	Chemical	Methacryloyl gelatin	Self cross-linking	$\sim$ 180	Open	54-82
[158]	Chemical	Polyacrylamide	N,N'-methylebebisacrylamide	200-1000 <sup>2</sup>	Open	
[118]	Chemical	Chitosan	Glyoxal	$\sim$ 1000 <sup>2</sup>	Closed	
[153]	Chemical	Poly(vinyl alcohol)	Glutaraldehyde	147 $\pm$ 17	Open	63
[159]	Physical + Chemical	Alginate	Calcium ions EDC/NHS	50-250	Open	63-83
[160]	Physical	Alginate	Calcium ions	31 $\pm$ 24	Open	93-96
[151]	Physical + Chemical	Alginate	Calcium ions EDC/NHS	100-200	Open	70
[161]	Physical + Chemical	Gelatin	Glutaraldehyde + Paraformaldehyde	60-90	Open	56-86

<sup>2</sup> Estimated optically from micrographs.

[162]	Chemical	Chitosan	Glyoxal	5-400	Open	
[40]	Physical	Gelatin	Self cross-linking	810 ± 30	Open	98

#### 4.2.2.2. Microfluidic foaming

Microfluidic foaming is a specific kind of gas injection in which a controlled flow of gas and liquid(s) flow are injected in a chip with micrometric channels to generate bubbles one by one (see Figure 9). If the gas and liquid flow rates are stable, the bubble formation is periodic, thus generating equal-size bubbles. One speaks then of a monodisperse foam. The monodisperse criterion is quantitatively set using the polydisperse index (PDI), which must be < 5% [24]. Monodisperse liquid foams tend to arrange in crystalline structures under the influence of gravity and confinement [24], an organisation that can be retained through solidification, as seen in Figure 10. The advantages of monodisperse foams are regularly exploited for model experiments in fundamental research [163,164]. For applications, monodisperse foams are particularly interesting for tissue engineering [153,155,156,161], or photonic/acoustic/mechanical metamaterials [162]. Microfluidic foaming also has the advantage that the highly controlled flow rates can be exploited to tune the final gel formulation.

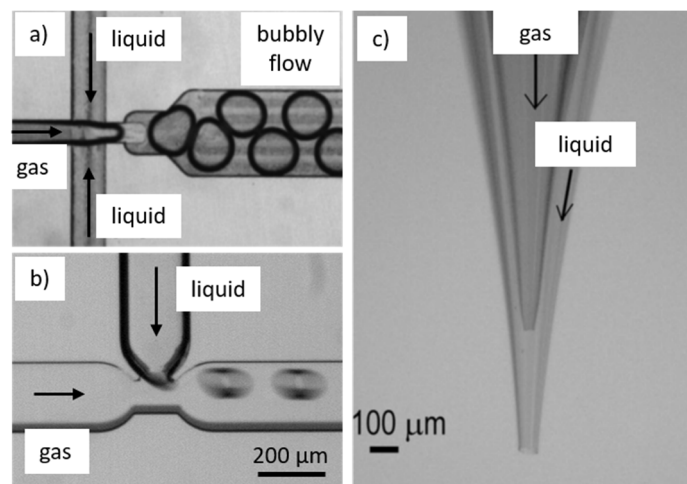


Figure 9: Different chip geometries used for microfluidic foaming. The arrows show the directions of the gas and liquid flows. a) Cross-flow geometry, adapted from [164]. b) T-Junction, adapted from [165]. c) Co-flow geometry, adapted from [160].

Different chip geometries exist to generate monodisperse bubbles, including cross-flow (Figure 9a), T-junctions (Figure 9b) or co-flow (Figure 9c). Other geometries exist, and we refer the reader to [29] for a more extensive list and the mechanisms behind bubble break-up. The choice of the geometry and the dimensions of the channels and constriction need to be thought carefully considering the bubble sizes aimed for, the accessible range of gas and liquid flow rates, and the viscoelastic properties of the foaming liquid. As such, for a given foaming liquid and flow geometry, a given range of bubble sizes – and thus pore sizes – is available [34,118,157,166].

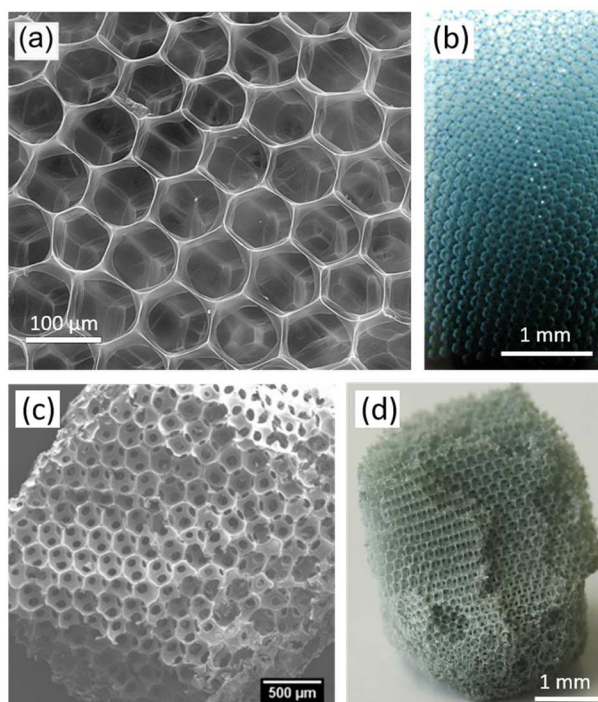


Figure 10: Examples of monodisperse hydrogel foams generated via microfluidic foaming. (a) Alginate foam cross-linked with calcium ions, from [155]. (b) Chitosan foam cross-linked with genipin, from [165]. (c) Freeze-dried gelatin methacryloyl foam, from [157]. (d) Freeze-dried chitosan cross-linked with genipin, from [34].

Microfluidic foam templating requires a careful tuning of the gel time to avoid blocking the microfluidic chip (long gel times) while optimising the stability of the liquid foam template (short gel times). Several cross-linking procedures exist to cope with these constraints (Figure 11a)).

- i) The cross-linker is mixed with the gelling polymer/monomer before injecting the liquid into the chip. This route requires either a very long cross-linking time (issues of foam stability may then arise) or the quenching of the cross-linking reaction by keeping the liquid container in an ice bath [32,162].
- ii) If the timescales for foaming and cross-linking are close, one can inject the cross-linker into the foam channel [34,118,154]. This requires precise control over the foaming and cross-linker flow rates to ensure a known and constant stoichiometric ratio of the monomer/polymer and cross-linker. Moreover, for highly viscous solutions, mixing the cross-linker with the foam is challenging as the liquids in a microfluidic chip flow with low Reynolds numbers, i.e., in a laminar regime, and mixing is essentially carried out by diffusion. Mixing units can be incorporated into the chip to mix liquids [41].
- iii) Finally, the foam can be generated without cross-linker and then cross-linked in an additional processing step. For example, the foam can be immediately frozen then freeze-dried to ensure its stability. The solid yet uncross-linked foam is then soaked in a cross-linker solution for a sufficient time to allow for a full cross-linking and is then freeze-dried again [151,153,159]. For systems with fast gelling kinetics (e.g., calcium-cross-linked alginate), the liquid foam can be directly cross-linked by pouring the cross-linker solution onto the foam [155]. Alternatively, the bubbles can

be collected directly into the cross-linker solution [156]. For systems in which cross-linking is initiated by UV irradiation, the foam can be collected into a transparent vial and then cross-linked by illuminating UV light on the sample [39,157]. However, since electromagnetic radiations are scattered by the foam interfaces, this cross-linking method limits the size of the foams that can be generated in a homogeneous manner.

- iv) Last but not least (Figure 11b), one can generate a stable precursor foam consisting only of water and surfactant and mix it with the monomer/polymer before applying the appropriate gelation trigger (pH, cross-linker, temperature, UV...) [40]. Note that this templating method involves a dilution of the monomer/polymer.

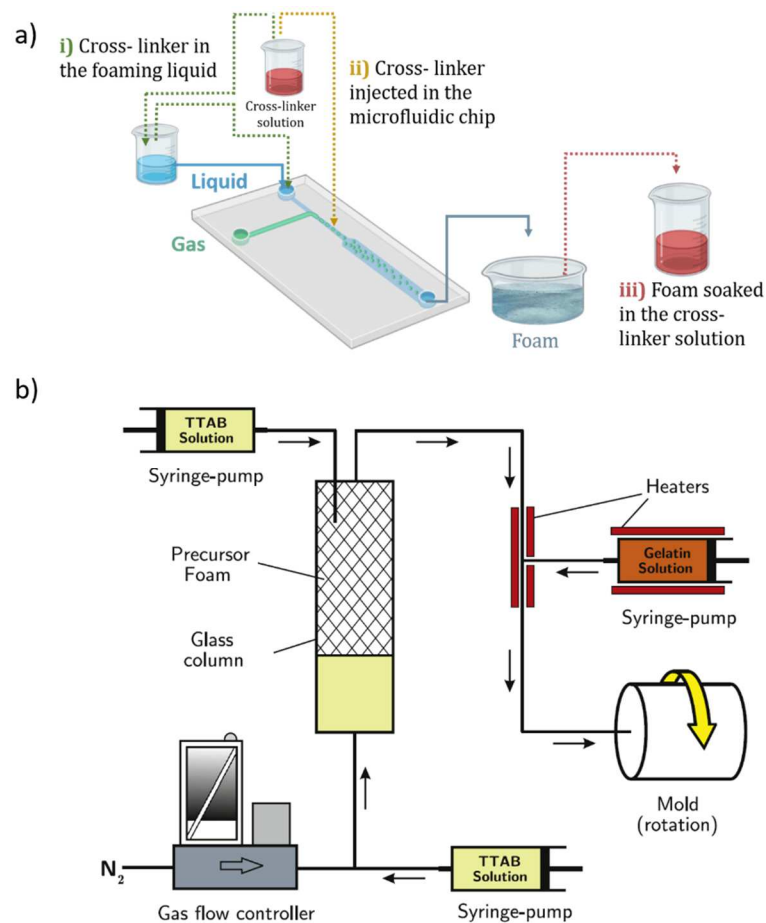


Figure 1: a) Scheme of microfluidic foam templating showing the possible alternatives for cross-linking. b) Alternative foam templating route in which the monodisperse liquid foam is a polymer-/monomer-free and is subsequently mixed with the gel-forming solution before subsequent gelation, from [40].

A known limitation of microfluidic foaming is the low foaming rate which rarely exceeds a few mL min<sup>-1</sup>. This is why much effort has been made to upscale microfluidics. While these efforts have been successful for droplet generation [60,167], they remain a challenge for bubble generation due to complex coupling phenomena introduced by the compressibility of the gas [168]. One of the most successful approaches seems to be step by step bubble generation [169]. An alternative to

microfluidic foaming yielding fairly monodisperse foams is membrane foaming. Similarly to batch gas injection described in Section 4.2.2.1, the membrane foaming cell consists of a paddle stirrer stirring the foaming liquid while gas is injected under a membrane with well-defined holes for bubble generation. This batch process can produce monodisperse foams (and emulsions) with throughputs of at least 400 mL h<sup>-1</sup> [170].

Microfluidic foaming can also be used to generate hydrogel foams with controlled polydispersity or property gradients using appropriate temporal variation of the chip geometry [33] or of the flow conditions [34].

## 5. Selected properties of hydrogel foams

### 5.1. Porosity and pore size

Since hydrogels commonly contain small amounts of polymer, their drying leads to the creation of a porous structure at the nano/micrometre scale. The type of structure which is obtained strongly depends on the drying process. For example, Figure 12d shows the typical example of a freeze-dried hydrogel. The porosity  $P$  is calculated from the ratio between the density of the dried porous gel  $\rho_G$  and of the polymer  $\rho_P$  [171]

$$P = \left(1 - \frac{\rho_G}{\rho_P}\right) \times 100. \quad (17)$$

The swollen state porosity can also be calculated as [172]

$$P_s = \left[1 - q_v \left(1 + \frac{(q_w - 1)d_2}{\rho_s}\right)^{-1}\right] \times 100, \quad (18)$$

where  $q_v$  is the equilibrium volume swelling ratio ( $V_w/V_{dry}$ ),  $q_w = (m_w/m_{dry})$ , and  $\rho_s$  is the density of the swelling solvent.

It is important here to distinguish between the porosity of the gel matrix and the foaming-induced porosity of the final hydrogel foam brought by gas introduction (Figure 1). The characteristic pore sizes of these two porosities have two very different length scales, the gel porosity being of the order of 1  $\mu\text{m}$  (fixed by the drying process) and the foam porosity being of the order of 100  $\mu\text{m}$  (fixed by the bubble size). This is why hydrogel foams are often called “superporous” hydrogels [10]. An illustrative example is shown in Figure 12. One also notices a pronounced difference in the properties of the same gel in bulk (Figure 12d) and in the foam (Figure 12c) [165]. It will be important to understand in what way this effect is related to the freeze-drying process or a confinement effect of the hydrogel between two liquid/gas interfaces. Globally, one should keep in mind that the bulk polymer network is likely to be different from the one within the foam.

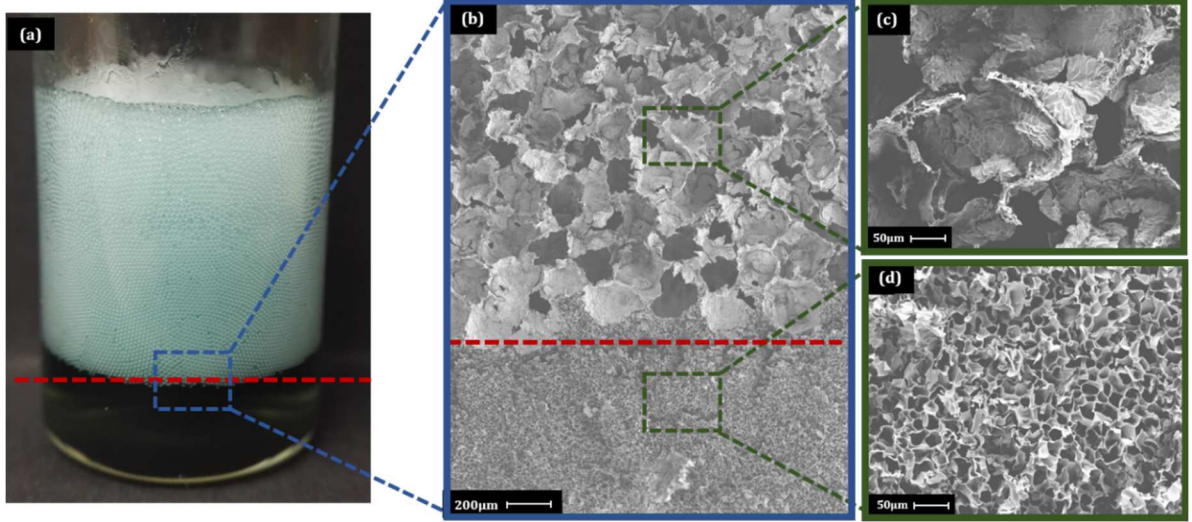


Figure 12: (a) A photograph of a monodisperse chitosan foam showing the foam on top and the drained gelled phase on the bottom separated by the red dashed line. (b) SEM micrograph of the same sample after freeze drying. (c) close-up SEM micrograph of the foam region. (d) close-up SEM micrograph of the drained phase. Adapted from [165].

## 5.2. Shear modulus

Unlike other types of solid foams, the shear modulus of hydrogel foams is commonly controlled by two contributions: the interfaces and the gelled continuous phase. The non-negligible contribution of the interface is due to the fact that (i) the surface tension of water is very high (0.072 N/m) even in presence of surfactants (0.03-0.05 N/m), and (ii) the elastic shear moduli of bulk hydrogels are commonly low (order of 10 kPa).

To a first approximation, the **contribution of the gel to the shear modulus of the foam** may be estimated via [64,173]

$$G_{\text{foam,g}}(\varphi) \sim \frac{9}{8} G_{\text{gel}}(1 - \varphi)^2. \quad (19)$$

Therefore, the solid contribution to the shear modulus strongly decreases with increasing gas fraction  $\varphi$  and depends linearly on the shear modulus  $G_{\text{gel}}$  of the continuous phase. Note that Equation (19) is not a simple mixture law but also takes into account the macroporous structure of foams as its application to the bulk hydrogel (i.e.,  $\varphi = 0$ ) does not give  $G_{\text{foam,g}} = G'_{\text{gel}}$ .

The **contribution of the interfaces to the shear modulus of the foam** results from the fact that a shearing action deforms the bubbles and hence increases their surface area (and hence the surface energy of the foam). This contribution may be estimated by [21,35,174]

$$G_{\text{foam,i}}(\varphi) = 2.4 \frac{\gamma}{d} \varphi(\varphi - \varphi_c). \quad (20)$$

One sees that this contribution is strongest for high gas fractions and strongly decreases as  $\varphi$  approaches  $\varphi_c$ . Note that since Equation (20) originates from the granular structure of foams, it is not defined for bubbly liquids, i.e., for  $\varphi < \varphi_c$ . One notices again the prefactor  $\gamma/d$  pointing out the importance of the bubble size.

In order to estimate the total shear modulus of the foam, one may be tempted to add both contributions. However, Gorlier et al. [175] showed that both terms are intrinsically coupled, since the bulk elasticity of the foam impacts how the interfaces are deformed. The authors show that the overall foam elasticity can be captured by a coupling term  $\psi$  so that

$$G_{\text{foam}} = G_{\text{foam,g}} + G_{\text{foam,i}} + \psi. \quad (21)$$

This coupling term depends on the elasto-capillary number of the foam, given by  $G_{\text{gel}}*d/\gamma$ , and on its gas fraction  $\varphi$ . This puts again in evidence the importance of the bubble size  $d$  and the gas fraction  $\varphi$ . These considerations do not replace accurate rheological measurements but give an insight into the key parameters which allow fine-tuning the shear elasticity of a hydrogel foam.

### 5.3. Pore connectivity

Pore connectivity is a crucial structural property of hydrogel foams since it allows gases, liquids, cells, etc. to propagate through the foam. It also sets many physical properties of the foam, including its mechanical [173] and acoustic properties [40]. For the particular case of cell culture and tissue engineering, the number and size of interconnections have a tremendous impact on cell growth related to cell migration and the facility with which nutrients and waste are transported throughout the material [176–178]. However, pore connectivity is still poorly controlled, and the detailed mechanisms responsible for the rupture of the thin films leading to pore opening remain to be understood. As of now, a very simple rule of thumbs allows for an approximate control of foam connectivity via foam templating. Globally one notices that apart from a few exceptions most hydrogel foams presented in the literature are open-cell (Table 2). This hints that in the case of hydrogel foams, polymers are either expelled from the thin films or the gelled films are so thin that they break upon drying. In this case, the pore opening corresponds to the zone of the thin films separating neighbouring bubbles in the liquid foam template, which has been confirmed by several authors [39,40]. This allows predicting how the diameter of the pore opening depends on the gas fraction and the foam structure [39,40,179,180]. For example, Figure 13 plots a theoretical prediction of how the ratio of the average pore opening diameter  $\langle d_w \rangle$  to the average pore diameter  $\langle d \rangle$  is expected to vary with the gas fraction  $\varphi$  (and the liquid fraction  $1-\varphi$ ) for monodisperse disordered foams (solid line) (from [179]). The dashed line is a computational prediction for a monodisperse ordered foam. The data (from [39]) are obtained for gelatin methacryloyl monodisperse foams which are partly ordered, hence expected to be in-between the theoretical and computational predictions.

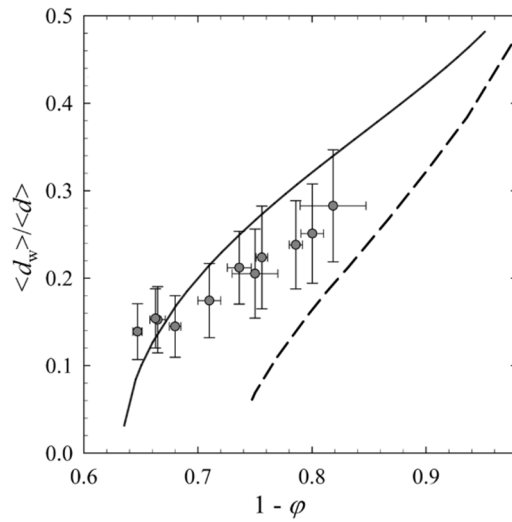


Figure 13: Ratio of average pore opening diameter  $d_w$  to average pore diameter  $d$  of gelatin methacryloyl monodisperse foams as a function of  $(1-\phi)$  compared with a model describing the film diameter for disordered monodisperse foams (continuous line, from [179]) and with surface evolver simulations for ordered, monodisperse foams (dashed line, from [163]). Adapted from [39].

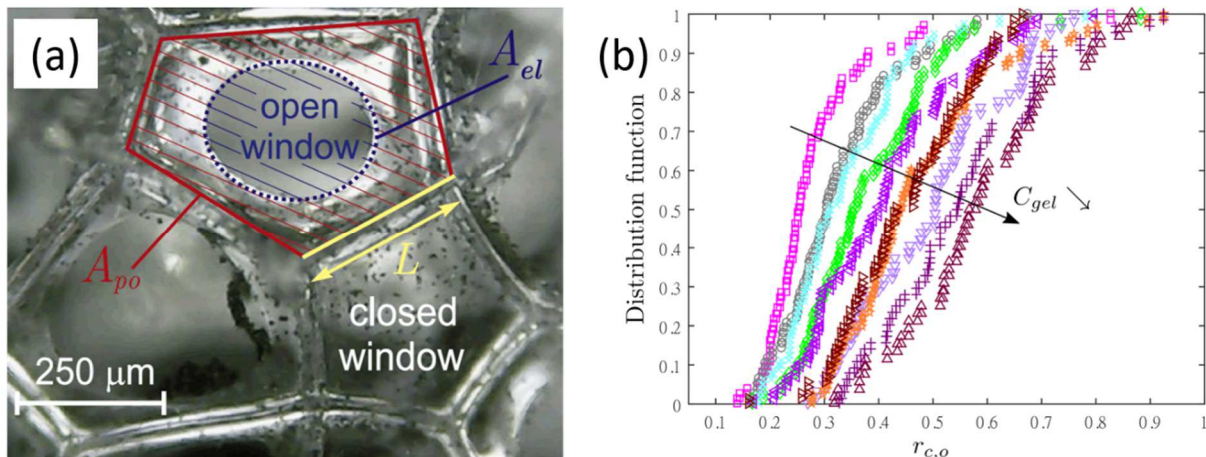


Figure 2: (a) Example of hydrogel foam bubble with open and closed pore windows (b) Probability to find a pore opening of radius  $r_{c,o}$  for increasing polymer concentration. Adapted from [40].

Isolated examples exist in which closed-cell hydrogel foams were obtained upon decreasing the gas fraction of the foam template [39,181] or increasing the monomer/polymer concentration in the foaming liquid [40]. In particular, Trinh et al. [40] showed how the probability of finding a pore opening of a given size decreases systematically with increasing gelatin concentration (Figure 14). I.e., the more solid content in the continuous phase, the more likely is the foam to have closed pores, i.e., the less likely are the thin films separating neighbouring pores to break. However, truly systematic studies of the thinning and rupture of thin films during gelation have yet to be conducted. Thin film rupture has been studied for *non-gelling* systems at the scale of isolated free-standing films [52,53,182,183] leading to the hypothesis that film rupture occurs when, due to film drainage, a critical film thickness is reached for which thermal fluctuations induce bursting. However, working with a gelling film, drainage may stop before the critical thickness for rupture has been reached, preventing its bursting. Moreover, the elasticity gained by the material through cross-linking may decrease the critical thickness for rupture, improving film stability. Systematic experimental investigations are still lacking to verify these assumptions, but recent instrumental developments allowing to monitor solidifying free-standing isolated films may advance the understanding of the rupture of gelling films, and thus pore opening mechanisms in hydrogel foams [184].

#### 5.4. Absorption capacity of hydrogel foams

The ability of dried hydrogels to absorb liquid is sought for many applications, such as decontamination or wound dressings. Two aspects are important in absorption applications: the *amount of absorbed liquid* and the *absorption speed*. For both aspects, open-cell hydrogel foams offer a great advantage due to their double porosity (Section 5.1) resulting from the foam pores ( $\sim 100 \mu\text{m}$ ) and the hydrogel pores ( $\sim 1 \mu\text{m}$ ) [10,25,28,185]. On the one hand, the foam pores offer additional void space, which can be filled by the absorbed liquid. On the other hand, an optimised foam structure may drastically increase the absorption rate during the imbibition process into the hydrogel foam. This “imbibition rate” is fixed by an equilibrium between the driving force (capillary suction) and the flow resistance [163], i.e., viscous dissipation [186]. The driving capillary suction depends on the wetting properties of the hydrogel surface, the surface tension of the liquid and on the size/shape of the pores. The resisting viscous dissipation depends on the viscosity of the absorbed liquid and the size and connectivity of the pores (Section 5.3). Globally, the smaller the pores, the stronger the driving force, but also the viscous dissipation. This contradicting influence of the pore size on both effects gives rise to an optimal pore size (and pore connectivity) for rapid

imbibition. Due to the very small pore size of dried non-foamed hydrogels, imbibition tends to be very slow. Using open-cell foams with appropriate pore dimensions and gas fractions, a first rapid imbibition occurs into the foam; the very large surface-to-volume ratio then allows for an efficient imbibition into the porous hydrogel. It is for the same reason that hydrogel beads have been used in the past for absorption applications, since a first rapid absorption arises into the spaces between the beads, from which the liquid then penetrates more slowly but efficiently into the beads thanks to their large surface area. Foams, however, have the advantage that they can be processed in one monolith. Figure 15 nicely illustrates the evolution of the absorption efficiency of hydrogel foams with increasing gas fraction for the example of poly(acrylamide-co-acrylic acid) foams [25]. While this general idea has been known for a long time, systematic investigations of the intricate interplay between imbibition and foam structure combining experiments, simulations and modelling are only beginning to emerge [163,186].

In closed-cell foams, absorption must occur entirely through the continuous gel phase without the possibility of replacing the gas contained in the pores. Due to the intricate porous network, closed-cell foams tend to be even less efficient than dried non-foamed hydrogels for absorption applications as fewer imbibition pathways are available for the liquid. They may, however, provide a mechanical softness to the dry hydrogel, which can be of interest for specific applications.

While hydrogels are commonly dried before their use for absorption applications, hydrogel foams can, in principle, also be used for absorption in the wet state, provided that the foam is open-cell. In the only example known to us [187], this was used for decontamination with PVA hydrogels which were dried after absorption of the decontaminants to reduce waste.

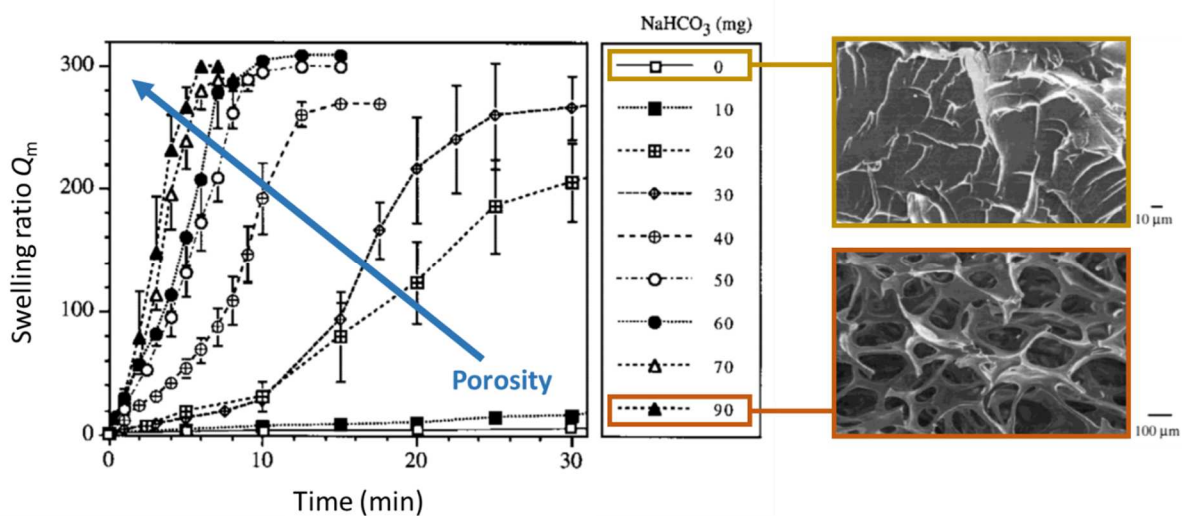


Figure 15: Evolution of swelling ratio  $Q_m$  with time for poly(acrylamide-co-acrylic acid) hydrogels with increasing porosity obtained through foaming. Adapted from [25].

The opposite process of hydrogel absorption is drying. Most hydrogel foams are used in a dried state with different requirements on the properties of the dried material. Often this concerns the mechanical properties of the dry foam in terms of integrity or softness, or the fact that a certain pore size needs to be maintained for optimal absorption capacities. However, many artefacts can arise during drying due to the significant shrinkage upon water removal. For example, internal stresses may rupture the gel or lead to complete foam collapse; or an open-cell foam may collapse under its own weight. Freeze-drying, which is often used for non-foamed hydrogels, also proceeds

very differently in foamed hydrogels. While drying effects have been investigated systematically for particulate hydrogel foams [188–190], polymeric hydrogel foams await systematic investigation.

## 6. Conclusion

While hydrogels have been used for decades, hydrogel foams have only recently started to make their way into applications despite their great promise in tuning their mechanical or absorption properties over a wide range. This delay is partly due to the challenge of matching foam and hydrogel formation, each process having its own characteristic timescales which are often controlled through the same formulation parameters in a conflicting manner. We therefore advocate here the approach of “liquid foam templating”, in which an initially liquid foam with controlled stability and morphology is gelled in a second step. As such, one can build on the vast scientific know-how established for liquid foams (generation, stability, structure) over the last 30 years. We summarised here some of the key elements to keep in mind during the formulation of hydrogel foams via liquid foam templating.

Hydrogel foams raise many interesting and challenging scientific questions, most of which still await to be tackled in a systematic manner. Some of the main questions include:

- (1) How does the foam influence the gelation process and the final gel properties in comparison to a bulk gel made with the same formulation?
- (2) Which mechanisms control the pore opening process in hydrogel foams?
- (3) How can the mechanical properties of the wet and dry foam be predicted?
- (4) How are foam structure and gel properties coupled in the drying and absorption processes? How can they be optimised?

While some of this know-how has been established for superabsorbing hydrogel foams due to their importance for hygiene applications, it remains in the hands of the concerned R&D departments. A profound academic understanding of the associated phenomena will, however, become of increasing importance to ensure the necessary flexibility to respond to increasingly strict environmental regulations. The increasing use of bio-derived polymers requires the development of reliable protocols despite the natural variability of the formulations.

While we concentrated here on “classic hydrogels” in order to maintain the focus on the foams, future work should, of course, combine the foam properties with the “modern” capacities of hydrogels (superabsorption, self-healing, hybrid-hydrogels, stimuli-responsiveness, drug delivery, etc.). It will be important to understand how the different hydrogel features translate to the overall foam properties.

While we discussed mostly how the foam will be useful for hydrogel applications, future work may treat the opposite question: how can hydrogel features be useful for foam applications? Classic hydrogel foams have already been exploited as metamaterials [162,191], and internal stresses or other gel features may be exploited to create novel types of foam structures with optimized metamaterial features.

While this review focuses on hydrogel foams, many non-aqueous gel systems await to be foamed. Moving away from water raises many challenging questions of current research as to finding appropriate stabilizing agents.

In summary, hydrogel foams will continue to offer an exciting playground for interdisciplinary work uniting chemists, physical chemists, physicists and biologists around a set of common fundamental and applied questions.

## 7. Acknowledgement

We acknowledge funding from the European Research Council (ERC-METAFOAM 819511) and from the region Grand-Est (“Soutien aux jeunes chercheurs” fellowship, S. Andrieux). We also acknowledge financial support from Urgo RID.

## 8. References

- [1] France KJ De, Xu F, Hoare T. Structured Macroporous Hydrogels: Progress, Challenges, and Opportunities. *Adv Healthc Mater* 2018;7:1700927. <https://doi.org/10.1002/ADHM.201700927>.
- [2] Conley Wake M, Mikos AG, Sarakinos G, Vacanti JP, Langer R. Dynamics of fibrovascular tissue ingrowth in hydrogel foams. *Cell Transplant* 1995;4:275–9. [https://doi.org/https://doi.org/10.1016/0963-6897\(95\)00003-G](https://doi.org/https://doi.org/10.1016/0963-6897(95)00003-G).
- [3] Andersen T, Markussen C, Dornish M, Heier-Baardson H, Melvik JE, Alsberg E, et al. In situ gelation for cell immobilization and culture in alginate foam scaffolds. *Tissue Eng - Part A* 2014. <https://doi.org/10.1089/ten.tea.2013.0223>.
- [4] Raya B, Caroline C, Christophe T, Benjamin D, Philippe B, Daniel C, et al. Design of biopolymer-based 3D scaffolds for cardiac mesenchymal stem cell therapy. *Front Bioeng Biotechnol* 2016. <https://doi.org/10.3389/conf.fbioe.2016.01.00734>.
- [5] Lundin JG, Daniels GC, McGann CL, Stanbro J, Watters C, Stockelman M, et al. Multi-Functional Polyurethane Hydrogel Foams with Tunable Mechanical Properties for Wound Dressing Applications. *Macromol Mater Eng* 2017;302.
- [6] Gorczyca G, Tylingo R, Szweda P, Augustin E, Sadowska M, Milewski S. Preparation and characterization of genipin cross-linked porous chitosan-collagen-gelatin scaffolds using chitosan-CO<sub>2</sub> solution. *Carbohydr Polym* 2014;102:901–11. <https://doi.org/http://dx.doi.org/10.1016/j.carbpol.2013.10.060>.
- [7] Aminabhavi TM, Deshmukh AS. *Polymeric Hydrogels as Smart Biomaterials*. 2016. <https://doi.org/10.1007/978-3-319-25322-0>.
- [8] Dubey S, Sharma R, Mody N, Vyas SP. *Polymeric Hydrogel: A Flexible Carrier System for Drug Delivery*, Springer, Singapore; 2018, p. 141–84. [https://doi.org/10.1007/978-981-10-6083-0\\_6](https://doi.org/10.1007/978-981-10-6083-0_6).
- [9] Silverstein MS, Cameron NR, Hillmyer MA. *Porous polymers*. John Wiley & Sons; 2011.
- [10] Omidian H, Rocca JG, Park K. Advances in superporous hydrogels. *J Control Release* 2005;102:3–12. <https://doi.org/https://doi.org/10.1016/j.jconrel.2004.09.028>.
- [11] Andrieux S, Quell A, Stubenrauch C, Drenckhan W. Liquid foam templating – A route to tailor-made polymer foams. *Adv Colloid Interface Sci* 2018;256:276–90. <https://doi.org/10.1016/J.CIS.2018.03.010>.
- [12] Stubenrauch C, Menner A, Bismarck A, Drenckhan W. Emulsion and Foam Templating- Promising Routes to Tailor-Made Porous Polymers. *Angew Chemie Int Ed* 2018;57:10024–32. <https://doi.org/10.1002/anie.201801466>.
- [13] Qian L, Ahmed A, Foster A, Rannard SP, Cooper AI, Zhang H. Systematic tuning of pore morphologies and pore volumes in macroporous materials by freezing. *J Mater Chem*

- 2009;19:5212–9. <https://doi.org/10.1039/B903461G>.
- [14] Martoia F, Cochereau T, Dumont PJJ, Orgéas L, Terrien M, Belgacem MN. Cellulose nanofibril foams: Links between ice-templating conditions, microstructures and mechanical properties. *Mater Des* 2016;104:376–91.
- [15] Ma PX, Choi J-W. Biodegradable Polymer Scaffolds with Well-Defined Interconnected Spherical Pore Network. *Tissue Eng* 2001;7:23.
- [16] Cameron NR. High internal phase emulsion templating as a route to well-defined porous polymers. *Polymer (Guildf)* 2005;46:1439–49.
- [17] Pulko I, Krajnc P. High Internal Phase Emulsion Templating -- A Path To Hierarchically Porous Functional Polymers. *Macromol Rapid Commun* 2012;33:1731–46. <https://doi.org/10.1002/marc.201200393>.
- [18] Zhang T, Sanguramath RA, Israel S, Silverstein MS. Emulsion Templating: Porous Polymers and Beyond. *Macromolecules* 2019;52:5445–79. <https://doi.org/10.1021/acs.macromol.8b02576>.
- [19] Kimmins SD, Cameron NR. Functional Porous Polymers by Emulsion Templating: Recent Advances. *Adv Funct Mater* 2011;21:211–25. <https://doi.org/10.1002/adfm.201001330>.
- [20] Exerowa D, (Eds.) PMK, Ekserova DR (Dochi R, Krugliakov PM (Petr M, DOTCHI EXEROWA PMKYA. *Foam and Foam Films, Theory, Experiment, Application*. Elsevier, Amsterdam; 1998.
- [21] Weaire DL, Hutzler S. *The physics of foams*. Clarendon Press; 1999.
- [22] Cantat I, Cohen-Addad S, Elias F, Graner F, Höhler R, Pitois O, et al. *Foams - Structure and Dynamics*. Oxford University Press, Oxford; 2013.
- [23] Pugh RJ. *Bubble and Foam Chemistry*. 2016. <https://doi.org/10.1017/cbo9781316106938>.
- [24] Drenckhan W, Langevin D. Monodisperse foams in one to three dimensions. *Curr Opin Colloid Interface Sci* 2010;15:341–58. <https://doi.org/https://doi.org/10.1016/j.cocis.2010.06.002>.
- [25] Chen J, Park H, Park K. Synthesis of superporous hydrogels: Hydrogels with fast swelling and superabsorbent properties. *J Biomed Mater Res* 1999;44:53–62. [https://doi.org/10.1002/\(SICI\)1097-4636\(199901\)44:1<53::AID-JBM6>3.0.CO;2-W](https://doi.org/10.1002/(SICI)1097-4636(199901)44:1<53::AID-JBM6>3.0.CO;2-W).
- [26] Kabiri K, Omidian H, Zohuriaan-Mehr MJ. Novel approach to highly porous superabsorbent hydrogels: synergistic effect of porogens on porosity and swelling rate. *Polym Int* 2003;52:1158–64.
- [27] Kabiri K, Zohuriaan-Mehr MJ. Porous Superabsorbent Hydrogel Composites: Synthesis, Morphology and Swelling Rate. *Macromol Mater Eng* 2004;289:653–61. <https://doi.org/https://doi.org/10.1002/mame.200400010>.
- [28] Kuang J, Yuk KY, Huh KM. Polysaccharide-based superporous hydrogels with fast swelling and superabsorbent properties. *Carbohydr Polym* 2011;83:284–90. <https://doi.org/https://doi.org/10.1016/j.carbpol.2010.07.052>.
- [29] Drenckhan W, Saint-Jalmes A. The science of foaming. *Adv Colloid Interface Sci* 2015;222:228–59. <https://doi.org/http://dx.doi.org/10.1016/j.cis.2015.04.001>.
- [30] Keskar V, Marion NW, Mao JJ, Gemeinhart RA. In vitro evaluation of macroporous hydrogels to facilitate stem cell infiltration, growth, and mineralization. *Tissue Eng - Part A* 2009;15:1695–707. <https://doi.org/10.1089/ten.tea.2008.0238>.
- [31] David D, Silverstein MS. Porous polyurethanes synthesized within high internal phase

- emulsions. *J Polym Sci A* 2009;47:5806–14. <https://doi.org/10.1002/pola.23624>.
- [32] Andrieux S, Drenckhan W, Stubenrauch C. Highly ordered biobased scaffolds: From liquid to solid foams. *Polymer (Guildf)* 2017;126:425–31. <https://doi.org/10.1016/j.polymer.2017.04.031>.
- [33] Costantini M, Jaroszewicz J, Kozoń Ł, Szlązak K, Świąszkowski W, Garstecki P, et al. 3D-Printing of Functionally Graded Porous Materials Using On-Demand Reconfigurable Microfluidics. *Angew Chemie - Int Ed* 2019;58:7620–5. <https://doi.org/10.1002/anie.201900530>.
- [34] Andrieux S, Drenckhan W, Stubenrauch C. Generation of Solid Foams with Controlled Polydispersity Using Microfluidics. *Langmuir* 2018;34:1581–90. <https://doi.org/10.1021/acs.langmuir.7b03602>.
- [35] Cantat I, Cohen-Addad S, Elias F, Graner FFF, Höhler R, Pitois O, et al. *Foams - Structure and Dynamics*. Oxford University Press, Oxford; 2013.
- [36] Drenckhan W, Hutzler S. Structure and energy of liquid foams. *Adv Colloid Interface Sci* 2015;224:1–16.
- [37] Forel E, Rio E, Schneider M, Beguin S, Weaire D, Hutzler S, et al. The surface tells it all: relationship between volume and surface fraction of liquid dispersions. *Soft Matter* 2016;12:8025–9. <https://doi.org/10.1039/C6SM01451H>.
- [38] Biance A-L, Delbos A, Pitois O. How Topological Rearrangements and Liquid Fraction Control Liquid Foam Stability. *Phys Rev Lett* 2011;106:68301. <https://doi.org/10.1103/PhysRevLett.106.068301>.
- [39] Dehli F, Southan A, Drenckhan W, Stubenrauch C. Tailoring and visualising pore openings in gelatin-based hydrogel foams. *J Colloid Interface Sci* 2020;588:326–35. <https://doi.org/10.1016/j.jcis.2020.12.064>.
- [40] Trinh VH, Langlois V, Guillemot J, Perrot C, Khidas Y, Pitois O. Tuning membrane content of sound absorbing cellular foams: Fabrication, experimental evidence and multiscale numerical simulations. *Mater Des* 2019;162:345–61. <https://doi.org/10.1016/j.matdes.2018.11.023>.
- [41] Testouri A, Ranft M, Honorez C, Kaabeche N, Ferbitz J, Freidank D, et al. Generation of Crystalline Polyurethane Foams Using Millifluidic Lab-on-a-Chip Technologies. *Adv Eng Mater* 2013;15:1086–98. <https://doi.org/10.1002/adem.201300077>.
- [42] S. Friberg HS. Foam stability and associated surfactants. In: Akers R, editor. *Foams*, London: Academic Press; 1976.
- [43] Guillermic RM, Salonen A, Emile J, Saint-Jalmes A. Surfactant foams doped with laponite: unusual behaviors induced by aging and confinement. *Soft Matter* 2009;5:4975. <https://doi.org/10.1039/b914923f>.
- [44] Varade D, Carriere D, Arriaga LR, Fameau A-L, Rio E, Langevin D, et al. On the origin of the stability of foams made from catanionic surfactant mixtures. *Soft Matter* 2011;7:6557. <https://doi.org/10.1039/c1sm05374d>.
- [45] Fameau A-L, Saint-Jalmes A, Cousin F, Houinsou Houssou B, Novales B, Navailles L, et al. Smart Foams: Switching Reversibly between Ultrastable and Unstable Foams. *Angew Chemie Int Ed* 2011;50:8264–9. <https://doi.org/10.1002/anie.201102115>.
- [46] Rio E, Drenckhan W, Salonen A, Langevin D. Unusually stable liquid foams. *Adv Colloid Interface Sci* 2014;205:74–86. <https://doi.org/http://dx.doi.org/10.1016/j.cis.2013.10.023>.

- [47] Maestro A, Drenckhan W, Rio E, Höhler R. Liquid dispersions under gravity: volume fraction profile and osmotic pressure. *Soft Matter* 2013;9:2531–40. <https://doi.org/10.1039/C2SM27668B>.
- [48] Cohen-Addad S, Höhler R, Pitois O. Flow in Foams and Flowing Foams. *Annu Rev Fluid Mech* 2013;45:241–67. <https://doi.org/10.1146/annurev-fluid-011212-140634>.
- [49] Guillermic R-M, Volland S, Faure S, Imbert B, Drenckhan W. Shaping complex fluids—How foams stand up for themselves. *J Rheol (N Y N Y)* 2013;57:333–48. <https://doi.org/10.1122/1.4769826>.
- [50] Hutzler S, Lösch D, Carey E, Weaire D, Hloucha M, Stubenrauch C. Evaluation of a steady-state test of foam stability. *Philos Mag* 2011;91:537–52. <https://doi.org/10.1080/14786435.2010.526646>.
- [51] Boos J, Drenckhan W, Stubenrauch C. Protocol for Studying Aqueous Foams Stabilized by Surfactant Mixtures. *J Surfactants Deterg* 2013;16:1–12. <https://doi.org/10.1007/s11743-012-1416-2>.
- [52] Rio E, Biance A-L. Thermodynamic and Mechanical Timescales Involved in Foam Film Rupture and Liquid Foam Coalescence. *ChemPhysChem* 2014;15:3692–707. <https://doi.org/10.1002/cphc.201402195>.
- [53] Chatzigiannakis E, Veenstra P, Ten Bosch D, Vermant J. Mimicking coalescence using a pressure-controlled dynamic thin film balance. *Soft Matter* 2020;16:9410–22. <https://doi.org/10.1039/d0sm00784f>.
- [54] Suja VC, Rodríguez-Hakim M, Tajuelo J, Fuller GG. Single bubble and drop techniques for characterizing foams and emulsions. *Adv Colloid Interface Sci* 2020;286:102295. <https://doi.org/10.1016/j.cis.2020.102295>.
- [55] Forel E, Dollet B, Langevin D, Rio E. Coalescence in Two-Dimensional Foams: A Purely Statistical Process Dependent on Film Area. *Phys Rev Lett* 2019;122:088002. <https://doi.org/10.1103/PhysRevLett.122.088002>.
- [56] Langevin D. Bubble coalescence in pure liquids and in surfactant solutions. *Curr Opin Colloid Interface Sci* 2015;20:92–7. <https://doi.org/10.1016/j.cocis.2015.03.005>.
- [57] Chan DYC, Klaseboer E, Manica R. Film drainage and coalescence between deformable drops and bubbles. *Soft Matter* 2011;7:2235–64. <https://doi.org/10.1039/c0sm00812e>.
- [58] Isert N, Maret G, Aegerter CM. Coarsening dynamics of three-dimensional levitated foams: From wet to dry. *Eur Phys J E* 2013;36:116. <https://doi.org/10.1140/epje/i2013-13116-x>.
- [59] Vignes-Adler M, Weaire D. New foams: Fresh challenges and opportunities. *Curr Opin Colloid Interface Sci* 2008;13:141–9. <https://doi.org/http://dx.doi.org/10.1016/j.cocis.2007.11.012>.
- [60] Nisisako T, Torii T. Microfluidic large-scale integration on a chip for mass production of monodisperse droplets and particles. *Lab Chip* 2008;8:287–93. <https://doi.org/10.1039/b713141k>.
- [61] Wang B, Prinsen P, Wang H, Bai Z, Wang H, Luque R, et al. Macroporous materials: Microfluidic fabrication, functionalization and applications. *Chem Soc Rev* 2017;46:855–914. <https://doi.org/10.1039/c5cs00065c>.
- [62] Weaire D, Pagonis V. Frustrated froth: Evolution of foam inhibited by an insoluble gaseous component. *Philos Mag Lett* 1990;62:417–21. <https://doi.org/10.1080/09500839008215544>.

- [63] Gandolfo FG, Rosano HL. Interbubble gas diffusion and the stability of foams. *J Colloid Interface Sci* 1997;194:31–6. <https://doi.org/10.1006/jcis.1997.5067>.
- [64] Bey H, Wintzenrieth F, Ronsin O, Höhler R, Cohen-Addad S. Stabilization of foams by the combined effects of an insoluble gas species and gelation. *Soft Matter* 2017;13:6816–30.
- [65] Andrieux S. Preliminary Work: From Liquid to Solid Foams. In: Andrieux S, editor., Cham: Springer International Publishing; 2019, p. 49–65. [https://doi.org/10.1007/978-3-030-27832-8\\_3](https://doi.org/10.1007/978-3-030-27832-8_3).
- [66] Tcholakova S, Mitrinova Z, Golemanov K, Denkov ND, Vethamuthu M, Ananthapadmanabhan KP. Control of Ostwald ripening by using surfactants with high surface modulus. *Langmuir* 2011;27:14807–19.
- [67] Tcholakova S, Mustan F, Pagureva N, Golemanov K, Denkov ND, Pelan EG, et al. Role of surface properties for the kinetics of bubble Ostwald ripening in saponin-stabilized foams. *Colloids Surfaces A Physicochem Eng Asp* 2017;534:16–25. <https://doi.org/10.1016/j.colsurfa.2017.04.055>.
- [68] Stocco A, Carriere D, Cottat M, Langevin D. Interfacial Behavior of Catanionic Surfactants. *Langmuir* 2010;26:10663–9. <https://doi.org/10.1021/la100954v>.
- [69] Maestro A, Rio E, Drenckhan W, Langevin D, Salonen A. Foams stabilised by mixtures of nanoparticles and oppositely charged surfactants: Relationship between bubble shrinkage and foam coarsening. *Soft Matter* 2014;10:6975–83. <https://doi.org/10.1039/c4sm00047a>.
- [70] Lucassen-Reynders E. Anionic surfactants: physical chemistry of surfactant action. New York: Dekker; 1981.
- [71] Kloek W, van Vliet T, Meinders M. Effect of Bulk and Interfacial Rheological Properties on Bubble Dissolution. *J Colloid Interface Sci* 2001;237:158–66. <https://doi.org/http://dx.doi.org/10.1006/jcis.2001.7454>.
- [72] Salonen A, Gay C, Maestro A, Drenckhan W, Rio E. Arresting bubble coarsening: A two-bubble experiment to investigate grain growth in the presence of surface elasticity. *EPL (Europhysics Lett)* 2016;116:46005. <https://doi.org/10.1209/0295-5075/116/46005>.
- [73] Jaensson N, Vermant J. Tensiometry and rheology of complex interfaces. *Curr Opin Colloid Interface Sci* 2018;37:136–50. <https://doi.org/10.1016/j.cocis.2018.09.005>.
- [74] Slaughter B V., Khurshid SS, Fisher OZ, Khademhosseini A, Peppas NA. Hydrogels in regenerative medicine. *Adv Mater* 2009;21:3307–29. <https://doi.org/10.1002/adma.200802106>.
- [75] Hu X, Li D, Zhou F, Gao C. Biological hydrogel synthesized from hyaluronic acid, gelatin and chondroitin sulfate by click chemistry. *Acta Biomater* 2011;7:1618–26. <https://doi.org/10.1016/j.actbio.2010.12.005>.
- [76] Wang Y, Xia S, Xiao G, Di J, Wang J. High-Loading Boron Nitride-Based Bio-Inspired Paper with Plastic-like Ductility and Metal-like Thermal Conductivity. *ACS Appl Mater Interfaces* 2020;12:13156–64. <https://doi.org/10.1021/acsami.9b21753>.
- [77] Mishra SB, Mishra AK. *Polymeric Hydrogels: A Review of Recent Developments*, Springer, Cham; 2016, p. 1–17. [https://doi.org/10.1007/978-3-319-25322-0\\_1](https://doi.org/10.1007/978-3-319-25322-0_1).
- [78] Zhang S, Nie Y, Tao H, Li Z. *Hydrogel-Based Strategies for Stem Cell Therapy*, 2018, p. 87–112. [https://doi.org/10.1007/978-981-10-6077-9\\_4](https://doi.org/10.1007/978-981-10-6077-9_4).

- [79] Venugopal JR, Sridhar S, Ramakrishna S. Electrospun plant-derived natural biomaterials for Tissue engineering. *Plant Sci Today* 2014;1:151–4. <https://doi.org/10.14719/pst.2014.1.3.65>.
- [80] Wang C, Stewart RJ, Kopeček J. Hybrid hydrogels assembled from synthetic polymers and coiled-coil protein domains. *Nature* 1999;397:417–20. <https://doi.org/10.1038/17092>.
- [81] Madhumitha G, Fowsiya J, Roopan SM. *Emerging Technology in Medical Applications of Hydrogel*, Springer, Singapore; 2018, p. 197–218. [https://doi.org/10.1007/978-981-10-6077-9\\_8](https://doi.org/10.1007/978-981-10-6077-9_8).
- [82] Dorkoosh FA, Borchard G, Rafiee-Tehrani M, Verhoef JC, Junginger HE. Evaluation of superporous hydrogel (SPH) and SPH composite in porcine intestine ex-vivo: Assessment of drug transport, morphology effect, and mechanical fixation to intestinal wall. *Eur J Pharm Biopharm* 2002;53:161–6. [https://doi.org/10.1016/S0939-6411\(01\)00222-3](https://doi.org/10.1016/S0939-6411(01)00222-3).
- [83] Mastropietro DJ, Omidian H, Park K. Drug delivery applications for superporous hydrogels. *Expert Opin Drug Deliv* 2012;9:71–89. <https://doi.org/10.1517/17425247.2012.641950>.
- [84] Aminabhavi TM, Deshmukh AS. *Polysaccharide-Based Hydrogels as Biomaterials*, Springer, Cham; 2016, p. 45–71. [https://doi.org/10.1007/978-3-319-25322-0\\_3](https://doi.org/10.1007/978-3-319-25322-0_3).
- [85] Thakur S, Thakur VK, Arotiba OA. *History, Classification, Properties and Application of Hydrogels: An Overview*, Springer, Singapore; 2018, p. 29–50. [https://doi.org/10.1007/978-981-10-6077-9\\_2](https://doi.org/10.1007/978-981-10-6077-9_2).
- [86] Braccini I, Pérez S. Molecular basis of Ca<sup>2+</sup>-induced gelation in alginates and pectins: The egg-box model revisited. *Biomacromolecules* 2001;2:1089–96. <https://doi.org/10.1021/bm010008g>.
- [87] Grant GT, Morris ER, Rees DA, Smith PJC, Thom D. Biological interactions between polysaccharides and divalent cations: The egg-box model. *FEBS Lett* 1973;32:195–8. [https://doi.org/10.1016/0014-5793\(73\)80770-7](https://doi.org/10.1016/0014-5793(73)80770-7).
- [88] Wang Z -Y, Zhang Q -Z, Konno M, Saito S. Sol–gel transition of alginate solution by the addition of various divalent cations: 13C-nmr spectroscopic study. *Biopolymers* 1993;33:703–11. <https://doi.org/10.1002/bip.360330419>.
- [89] Hoare TR, Kohane DS. Hydrogels in drug delivery: Progress and challenges. *Polymer (Guildf)* 2008;49:1993–2007. <https://doi.org/10.1016/j.polymer.2008.01.027>.
- [90] Xiong XY, Tam KC, Gan LH. Polymeric nanostructures for drug delivery applications based on pluronic copolymer systems. *J. Nanosci. Nanotechnol.*, vol. 6, 2006, p. 2638–50. <https://doi.org/10.1166/jnn.2006.449>.
- [91] Bohidar H, Saxena A, Tahir A, Kaloti M, Ali J. Effect of agar-gelatin compositions on the release of salbutamol tablets. *Int J Pharm Investig* 2011;1:93. <https://doi.org/10.4103/2230-973x.82407>.
- [92] Singh T, Laverty G, Donnelly R. *Hydrogels: design, synthesis and application in drug delivery and regenerative medicine*. 2018.
- [93] Zhang X, Zhao C, Xiang N, Li W. Chain Entanglements and Hydrogen Bonds in Carbopol Microgel Reinforced Hydrogel. *Macromol Chem Phys* 2016;217:2139–44. <https://doi.org/10.1002/macp.201600245>.
- [94] Thomas V, Yallapu MM, Sreedhar B, Bajpai SK. A versatile strategy to fabricate hydrogel-silver nanocomposites and investigation of their antimicrobial activity. *J Colloid Interface Sci* 2007;315:389–95. <https://doi.org/10.1016/j.jcis.2007.06.068>.

- [95] Achar L, Peppas NA. Preparation, characterization and mucoadhesive interactions of poly (methacrylic acid) copolymers with rat mucosa. *J Control Release* 1994;31:271–6. [https://doi.org/10.1016/0168-3659\(94\)90009-4](https://doi.org/10.1016/0168-3659(94)90009-4).
- [96] Nshyam S Chauha G, Kaur I, Misra BN. Modification of natural polymers: Part I-Ceric ion initiated graft copolymerization of methyl methacrylate onto Cannabis fibre. vol. 24. 1999.
- [97] Chan AW, Whitney RA, Neufeld RJ. Semisynthesis of a controlled stimuli-responsive alginate hydrogel. *Biomacromolecules* 2009;10:609–16. <https://doi.org/10.1021/bm801316z>.
- [98] Mirzaei B. E, Ramazani S. A. A, Shafiee M, Danaei M. Studies on Glutaraldehyde Crosslinked Chitosan Hydrogel Properties for Drug Delivery Systems. *Int J Polym Mater* 2013;62:605–11. <https://doi.org/10.1080/00914037.2013.769165>.
- [99] Bhattarai N, Gunn J, Zhang M. Chitosan-based hydrogels for controlled, localized drug delivery. *Adv Drug Deliv Rev* 2010;62:83–99.
- [100] Lee KY, Bouhadir KH, Mooney DJ. Controlled degradation of hydrogels using multi-functional cross-linking molecules. *Biomaterials* 2004. <https://doi.org/10.1016/j.biomaterials.2003.09.030>.
- [101] Cheng Y, Nada AA, Valmikinathan CM, Lee P, Liang D, Yu X, et al. In situ gelling polysaccharide-based hydrogel for cell and drug delivery in tissue engineering. *J Appl Polym Sci* 2014;131:n/a-n/a. <https://doi.org/10.1002/app.39934>.
- [102] Jeon O, Bouhadir KH, Mansour JM, Alsberg E. Photocrosslinked alginate hydrogels with tunable biodegradation rates and mechanical properties. *Biomaterials* 2009;30:2724–34. <https://doi.org/10.1016/j.biomaterials.2009.01.034>.
- [103] Jameela SR, Lakshmi S, James NR, Jayakrishnan A. Preparation and evaluation of photocrosslinkable chitosan as a drug delivery matrix. *J Appl Polym Sci* 2002;86:1873–7. <https://doi.org/10.1002/app.11112>.
- [104] Luo F, Sun TL, Nakajima T, Kurokawa T, Li X, Guo H, et al. Tough polyion-complex hydrogels from soft to stiff controlled by monomer structure. *Polymer (Guildf)* 2017;116:487–97. <https://doi.org/10.1016/j.polymer.2017.02.042>.
- [105] Kim GO, Kim N, Kim DY, Kwon JS, Min BH. An electrostatically crosslinked chitosan hydrogel as a drug carrier. *Molecules* 2012;17:13704–11. <https://doi.org/10.3390/molecules171213704>.
- [106] Draget K, Østgaard K, Polymers OS-C, 1990 U. Homogeneous alginate gels: A technical approach. Elsevier 1990.
- [107] Takamura A, Ishii F, Hidaka H. Drug release from poly(vinyl alcohol) gel prepared by freeze-thaw procedure. *J Control Release* 1992;20:21–7. [https://doi.org/10.1016/0168-3659\(92\)90135-E](https://doi.org/10.1016/0168-3659(92)90135-E).
- [108] Eagland D, Crowther NJ, Butler CJ. Complexation between polyoxyethylene and polymethacrylic acid-the importance of the molar mass of polyoxyethylene. *Eur Polym J* 1994;30:767–73. [https://doi.org/10.1016/0014-3057\(94\)90003-5](https://doi.org/10.1016/0014-3057(94)90003-5).
- [109] Ricciardi R, Gaillet C, Ducouret G, Polymer FL-, 2003 undefined. Investigation of the relationships between the chain organization and rheological properties of atactic poly (vinyl alcohol) hydrogels. Elsevier n.d.
- [110] Thomas S, Durand D, Chassenieux C, Jyotishkumar P. Handbook of Biopolymer-Based Materials. Weinheim, Germany: Wiley-VCH Verlag GmbH & Co. KGaA; 2013.

- <https://doi.org/10.1002/9783527652457>.
- [111] Dominguez J, ... BM the RIS on, 2013 U. Determination of the gel point of a polyfurfuryl alcohol resin and characterization of its curing rheokinetics. CoreAcUk n.d.
- [112] Raghavan SR, Chen LA, McDowell C, Khan SA, Hwang R, White S. Rheological study of crosslinking and gelation in chlorobutyl elastomer systems. *Polymer (Guildf)* 1996;37:5869–75. [https://doi.org/10.1016/S0032-3861\(96\)00446-6](https://doi.org/10.1016/S0032-3861(96)00446-6).
- [113] Tung CM, Dynes PJ. Relationship between viscoelastic properties and gelation in thermosetting systems. *J Appl Polym Sci* 1982;27:569–74. <https://doi.org/10.1002/app.1982.070270220>.
- [114] Winter HH. Can the gel point of a cross-linking polymer be detected by the  $G' - G''$  crossover? *Polym Eng Sci* 1987;27:1698–702. <https://doi.org/10.1002/pen.760272209>.
- [115] Suman K, Joshi YM. On the universality of the scaling relations during sol-gel transition. *J Rheol (N Y N Y)* 2020. <https://doi.org/10.1122/1.5134115>.
- [116] Chambon F, Winter HH. Linear Viscoelasticity at the Gel Point of a Crosslinking PDMS with Imbalanced Stoichiometry. *J Rheol (N Y N Y)* 1987;31:683–97. <https://doi.org/10.1122/1.549955>.
- [117] Winter HH, Chambon F. Analysis of Linear Viscoelasticity of a Crosslinking Polymer at the Gel Point. *J Rheol (N Y N Y)* 1986;30:367–82. <https://doi.org/10.1122/1.549853>.
- [118] Testouri A, Honorez C, Barillec A, Langevin D, Drenckhan W. Highly structured foams from chitosan gels. *Macromolecules* 2010;43:6166–73.
- [119] Michon C. Physical Gels of Biopolymers: Structure, Rheological and Gelation Properties. *Handb. Biopolym. Mater.*, Weinheim, Germany: Wiley-VCH Verlag GmbH & Co. KGaA; 2013, p. 699–716. <https://doi.org/10.1002/9783527652457.ch23>.
- [120] Behraves E, Jo S, Zygourakis K, Mikos AG. Synthesis of in Situ Cross-Linkable Macroporous Biodegradable Hydrogels. *Biomacromolecules* 2002;3:374–81. <https://doi.org/10.1021/bm010158r>.
- [121] Ramdhan T, Ching SH, Prakash S, Bhandari B. Time dependent gelling properties of cuboid alginate gels made by external gelation method: Effects of alginate-CaCl<sub>2</sub> solution ratios and pH. *Food Hydrocoll* 2019;90:232–40. <https://doi.org/10.1016/j.foodhyd.2018.12.022>.
- [122] Catanzano O, Soriente A, La Gatta A, Cammarota M, Ricci G, Fasolino I, et al. Macroporous alginate foams crosslinked with strontium for bone tissue engineering. *Carbohydr Polym* 2018;202:72–83. <https://doi.org/10.1016/j.carbpol.2018.08.086>.
- [123] Ashida K. *Polyurethane and Related Foams*. CRC Press; 2006. <https://doi.org/10.1201/9780203505991>.
- [124] Cho YS, Lee JW, Lee JS, Lee JH, Yoon TR, Kuroyanagi Y, et al. Hyaluronic acid and silver sulfadiazine-impregnated polyurethane foams for wound dressing application. *J Mater Sci Mater Med* 2002;13:861–5. <https://doi.org/10.1023/A:1016500429225>.
- [125] Sannino A, Netti PA, Madaghiele M, Coccoli V, Luciani A, Maffezzoli A, et al. Synthesis and characterization of macroporous poly(ethylene glycol)-based hydrogels for tissue engineering application. *J Biomed Mater Res Part A* 2006;79A:229–36. <https://doi.org/10.1002/jbm.a.30780>.
- [126] Poursamar SA, Hatami J, Lehner AN, Da Silva CL, Ferreira FC, Antunes APM. Gelatin porous

- scaffolds fabricated using a modified gas foaming technique: Characterisation and cytotoxicity assessment. *Mater Sci Eng C* 2015;48:63–70. <https://doi.org/10.1016/j.msec.2014.10.074>.
- [127] Barbetta A, Barigelli E, Dentini M. Porous Alginate Hydrogels: Synthetic Methods for Tailoring the Porous Texture. *Biomacromolecules* 2009;10:2328–37. <https://doi.org/10.1021/bm900517q>.
- [128] Cole SM, Garbe JE, Woodson LP. Water-insoluble polysaccharide hydrogel foam for medical applications, 1992.
- [129] Park H, Park K, Kim D. Preparation and swelling behavior of chitosan-based superporous hydrogels for gastric retention application. *J Biomed Mater Res - Part A* 2006;76:144–50. <https://doi.org/10.1002/jbm.a.30533>.
- [130] Chen S, Zhou B, Ma M, Wu B, Shi Y, Wang X. Multiporous microstructure for enhancing the water absorption and swelling rate in poly(sodium acrylic acid) superabsorbent hydrogels based on a novel physical and chemical composite foaming system. *J Appl Polym Sci* 2016;133. <https://doi.org/10.1002/app.44149>.
- [131] Chavda H V, Patel CN, Karen HD. Preparation and characterization of chitosan-based superporous hydrogel composite. *J Young Pharm* 2009;1:199–204. <https://doi.org/10.4103/0975-1483.57064>.
- [132] Barbetta A, Gumiero A, Pecci R, Bedini R, Dentini M. Gas-in-liquid foam templating as a method for the production of highly porous scaffolds. *Biomacromolecules* 2009;10:3188–92.
- [133] Tang Y, Lin S, Yin S, Jiang F, Zhou M, Yang G, et al. In situ gas foaming based on magnesium particle degradation: A novel approach to fabricate injectable macroporous hydrogels. *Biomaterials* 2020;232. <https://doi.org/10.1016/j.biomaterials.2019.119727>.
- [134] Topuz F, Henke A, Richtering W, Groll J. Magnesium ions and alginate do form hydrogels: A rheological study. *Soft Matter* 2012;8:4877–81. <https://doi.org/10.1039/c2sm07465f>.
- [135] Stehr J. Chemical blowing agents in the rubber industry. Past - present - and future? *Int Polym Sci Technol* 2016;43:812–9. <https://doi.org/10.1177/0307174x1604300501>.
- [136] Omidian H, Yasger PD. United States US 20080206339A1 (12) Patent Application Publication (10) Pub. vol. 28. 2008.
- [137] Deleurence R, Saison T, Lequeux F, Monteux C. Time scales for drainage and imbibition in gellified foams: Application to decontamination processes. *Soft Matter* 2015;11:7032–7. <https://doi.org/10.1039/c5sm01158b>.
- [138] Deleurence R, Saison T, Lequeux F, Monteux C. Foaming of Transient Polymer Hydrogels. *ACS Omega* 2018;3:1864–70. <https://doi.org/10.1021/acsomega.7b01301>.
- [139] Andersen T, Melvik JE, Gåserød O, Alsberg E, Christensen BE. Ionically Gelled Alginate Foams: Physical Properties Controlled by Operational and Macromolecular Parameters. *Biomacromolecules* 2012;13:3703–10. <https://doi.org/10.1021/bm301194f>.
- [140] Tan H, Tu S, Zhao Y, Wang H, Du Q. A simple and environment-friendly approach for synthesizing macroporous polymers from aqueous foams. *J Colloid Interface Sci* 2018;509:209–18. <https://doi.org/10.1016/j.jcis.2017.09.018>.
- [141] Hsieh W-C, Chang C-P, Lin S-M. Morphology and characterization of 3D micro-porous structured chitosan scaffolds for tissue engineering. *Colloids Surfaces B Biointerfaces* 2007;57:250–5. <https://doi.org/10.1016/J.COLSURFB.2007.02.004>.

- [142] Gaillard T, Roché M, Honorez C, Jumeau M, Balan A, Jedrzejczyk C, et al. Controlled foam generation using cyclic diphasic flows through a constriction. *Int J Multiph Flow* 2017;96:173–87.
- [143] Zowada R, Foudazi R. Polyfoam: Foam-Templated Microcellular Polymers. *Langmuir* 2020;36:7868–78. <https://doi.org/10.1021/acs.langmuir.0c00932>.
- [144] Mansur HS, Costa HS. Nanostructured poly(vinyl alcohol)/bioactive glass and poly(vinyl alcohol)/chitosan/bioactive glass hybrid scaffolds for biomedical applications. *Chem Eng J* 2008;137:72–83. <https://doi.org/http://dx.doi.org/10.1016/j.cej.2007.09.036>.
- [145] Lan G, Lu B, Wang T, Wang L, Chen J, Yu K, et al. Chitosan/gelatin composite sponge is an absorbable surgical hemostatic agent. *Colloids Surfaces B Biointerfaces* 2015;136:1026–34. <https://doi.org/10.1016/j.colsurfb.2015.10.039>.
- [146] Ceccaldi C, Bushkalova R, Cussac D, Duployer B, Tenailleau C, Bourin P, et al. Elaboration and evaluation of alginate foam scaffolds for soft tissue engineering Elaboration and evaluation of alginate foam scaffolds for soft tissue engineering Elaboration and evaluation of alginate foam scaffolds for soft tissue engineering *Open Arch. Int J Pharm* 2017;524:433–42. <https://doi.org/10.1016/j.ijpharm.2017.02.060>.
- [147] Andersen T, Melvik JE, Gåserød O, Alsberg E, Christensen BE. Ionically gelled alginate foams: Physical properties controlled by type, amount and source of gelling ions. *Carbohydr Polym* 2014;99:249–56. <https://doi.org/https://doi.org/10.1016/j.carbpol.2013.08.036>.
- [148] Nilsen-Nygaard J, Hattrem MN, Draget KI. Propylene glycol alginate (PGA) gelled foams: A systematic study of surface activity and gelling properties as a function of degree of esterification. *Food Hydrocoll* 2016;57:80–91. <https://doi.org/10.1016/J.FOODHYD.2016.01.011>.
- [149] Barbetta A, Rizzitelli G, Bedini R, Pecci R, Dentini M. Porous gelatin hydrogels by gas-in-liquid foam templating. *Soft Matter* 2010;6:1785–92.
- [150] Barbetta A, Carrino A, Costantini M, Dentini M. Polysaccharide based scaffolds obtained by freezing the external phase of gas-in-liquid foams. *Soft Matter* 2010;6:5213–24. <https://doi.org/10.1039/C0SM00616E>.
- [151] Costantini M, Colosi C, Mozetic P, Jaroszewicz J, Tosato A, Rainer A, et al. Correlation between porous texture and cell seeding efficiency of gas foaming and microfluidic foaming scaffolds. *Mater Sci Eng, C* 2016;62:668–77. <https://doi.org/http://dx.doi.org/10.1016/j.msec.2016.02.010>.
- [152] Chimenti I, Rizzitelli G, Gaetani R, Angelini F, Ionta V, Forte E, et al. Human cardiosphere-seeded gelatin and collagen scaffolds as cardiogenic engineered bioconstructs. *Biomaterials* 2011;32:9271–81. <https://doi.org/10.1016/j.biomaterials.2011.08.049>.
- [153] Colosi C, Costantini M, Barbetta A, Pecci R, Bedini R, Dentini M. Morphological Comparison of PVA Scaffolds Obtained by Gas Foaming and Microfluidic Foaming Techniques. *Langmuir* 2013;29:82–91. <https://doi.org/10.1021/la303788z>.
- [154] Andrieux S, Medina L, Herbst M, Berglund LALA, Stubenrauch C. Monodisperse highly ordered chitosan/cellulose nanocomposite foams. *Compos Part A Appl Sci Manuf* 2019;125:105516. <https://doi.org/10.1016/j.compositesa.2019.105516>.
- [155] Chung K, Mishra NC, Wang C, Lin F, Lin K. Fabricating scaffolds by microfluidics. *Biomicrofluidics* 2009;3:22403.

- [156] Wang C-C, Yang K-C, Lin K-H, Liu H-C, Lin F-H. A highly organized three-dimensional alginate scaffold for cartilage tissue engineering prepared by microfluidic technology. *Biomaterials* 2011;32:7118–26. <https://doi.org/10.1016/J.BIOMATERIALS.2011.06.018>.
- [157] Dehli F, Rebers L, Stubenrauch C, Southan A. Highly Ordered Gelatin Methacryloyl Hydrogel Foams with Tunable Pore Size. *Biomacromolecules* 2019;20:2666–74. <https://doi.org/10.1021/acs.biomac.9b00433>.
- [158] van der Net A, Gryson A, Ranft M, Elias F, Stubenrauch C, Drenckhan W. Highly structured porous solids from liquid foam templates. *Colloids Surfaces A Physicochem Eng Asp* 2009;346:5–10.
- [159] Costantini M, Colosi C, Jaroszewicz J, Tosato A, Świążkowski W, Dentini M, et al. Microfluidic Foaming: A Powerful Tool for Tailoring the Morphological and Permeability Properties of Sponge-like Biopolymeric Scaffolds. *ACS Appl Mater Interfaces* 2015;7:23660–71. <https://doi.org/10.1021/acsami.5b08221>.
- [160] Ahmad B, Stride E, Edirisinghe M. Calcium Alginate Foams Prepared by a Microfluidic T-Junction System: Stability and Food Applications. *Food Bioprocess Technol* 2012;5:2848–57. <https://doi.org/10.1007/s11947-011-0650-3>.
- [161] Lin J, Lin W, Hong W, Hung W, Nowotarski SH, Gouveia SM, et al. Morphology and organization of tissue cells in 3D microenvironment of monodisperse foam scaffolds. *Soft Matter* 2011;7:10010–6. <https://doi.org/10.1039/C1SM05371J>.
- [162] Maimouni I, Morvaridi M, Russo M, Lui G, Morozov K, Cossy J, et al. Micrometric Monodisperse Solid Foams as Complete Photonic Bandgap Materials. *ACS Appl Mater Interfaces* 2020;12:32061–8. <https://doi.org/10.1021/acsami.0c04031>.
- [163] Pitois O, Kaddami A, Langlois V. Capillary imbibition in open-cell monodisperse foams. *J Colloid Interface Sci* 2020. <https://doi.org/10.1016/j.jcis.2020.03.013>.
- [164] Spadoni A, Höhler R, Cohen-Addad S, Dorodnitsyn V. Closed-cell crystalline foams: Self-assembling, resonant metamaterials. *J Acoust Soc Am* 2014;135:1692–9. <https://doi.org/10.1121/1.4867375>.
- [165] Andrieux S. *Monodisperse Highly Ordered and Polydisperse Biobased Solid Foams*. Cham: Springer International Publishing; 2019. <https://doi.org/10.1007/978-3-030-27832-8>.
- [166] Dabrowski ML, Stubenrauch C. Methacrylate-Based Polymer Foams with Controllable Pore Sizes and Controllable Polydispersities via Foamed Emulsion Templating. *Adv Eng Mater* 2020;2001013. <https://doi.org/10.1002/adem.202001013>.
- [167] Nisisako T, Ando T, Hatsuzawa T. High-volume production of single and compound emulsions in a microfluidic parallelization arrangement coupled with coaxial annular world-to-chip interfaces. *Lab Chip* 2012;12:3426–35.
- [168] Hashimoto M, Shevkoplyas SS, Zasońska B, Szyborski T, Garstecki P, Whitesides GM. Formation of Bubbles and Droplets in Parallel, Coupled Flow-Focusing Geometries. *Small* 2008;4:1795–805. <https://doi.org/10.1002/smll.200800591>.
- [169] van Dijke KC, Schroën K, van der Padt A, Boom R. EDGE emulsification for food-grade dispersions. *J Food Eng* 2010. <https://doi.org/10.1016/j.jfoodeng.2009.10.028>.
- [170] Carballido L, Dabrowski ML, Dehli F, Koch L, Stubenrauch C. Monodisperse liquid foams via membrane foaming. *J Colloid Interface Sci* 2020;568:46–53. <https://doi.org/10.1016/j.jcis.2020.02.036>.

- [171] Dinu MV, Ozmen MM, Dragan ES, Okay O. Freezing as a path to build macroporous structures: Superfast responsive polyacrylamide hydrogels. *Polymer (Guildf)* 2007;48:195–204. <https://doi.org/10.1016/j.polymer.2006.11.022>.
- [172] Ozmen MM, Dinu MV, Dragan ES, Okay O. Preparation of Macroporous Acrylamide-based Hydrogels: Cryogelation under Isothermal Conditions. *J Macromol Sci Part A* 2007;44:1195–202. <https://doi.org/10.1080/10601320701561148>.
- [173] Gibson LJ, Ashby MF. *Cellular Solids: Structure and Properties* (Cambridge Solid State Science Series). 2nd ed. Cambridge University Press, Cambridge; 1997.
- [174] Saint-Jalmes A, Durian DJ. Vanishing elasticity for wet foams: Equivalence with emulsions and role of polydispersity. *J Rheol (N Y N Y)* 1999;43:1411–22. <https://doi.org/10.1122/1.551052>.
- [175] Gorlier F, Khidas Y, Pitois O. Coupled elasticity in soft solid foams. *J Colloid Interface Sci* 2017;501:103–11.
- [176] Hutmacher DW. Scaffolds in tissue engineering bone and cartilage. *Biomaterials* 2000;21:2529–43. [https://doi.org/10.1016/S0142-9612\(00\)00121-6](https://doi.org/10.1016/S0142-9612(00)00121-6).
- [177] Karp JM, Dalton PD, Shoichet MS. Scaffolds for Tissue Engineering. *MRS Bull* 2003;28:301–6. <https://doi.org/10.1557/mrs2003.85>.
- [178] Lutzweiler G, Barthes J, Koenig G, Kerdjoudj H, Mayingi J, Boulmedais F, et al. Modulation of Cellular Colonization of Porous Polyurethane Scaffolds via the Control of Pore Interconnection Size and Nanoscale Surface Modifications. *ACS Appl Mater Interfaces* 2019;11:19819–29. <https://doi.org/10.1021/acsami.9b04625>.
- [179] Princen HM. Pressure/Volume/Surface Area Relationships in Foams and Highly Concentrated Emulsions: Role of Volume Fraction. *Langmuir* 1988;4:164–9. <https://doi.org/10.1021/la00079a030>.
- [180] Arditty S, Schmitt V, Lequeux F, Leal-Calderon F. Interfacial properties in solid-stabilized emulsions. *Eur Phys J B* 2005;44:381–93. <https://doi.org/10.1140/epjb/e2005-00137-0>.
- [181] Testouri A, Arriaga LR, Honorez C, Ranft M, Rodrigues J, van der Net A, et al. Generation of porous solids with well-controlled morphologies by combining foaming and flow chemistry on a Lab-on-a-Chip. *Colloids Surfaces A Physicochem Eng Asp* 2012;413:17–24.
- [182] Petit PC, Le Merrer M, Biance AL. Holes and cracks in rigid foam films. *J Fluid Mech* 2015. <https://doi.org/10.1017/jfm.2015.278>.
- [183] Chatzigiannakis E, Vermant J. Breakup of Thin Liquid Films: From Stochastic to Deterministic. *Phys Rev Lett* 2020;125:158001. <https://doi.org/10.1103/PhysRevLett.125.158001>.
- [184] Andrieux S, Muller P, Kaushal M, Macias Vera NS, Bollache R, Honorez C, et al. Microfluidic thin film pressure balance for the study of complex thin films. *Lab Chip* 2021;21:412–20. <https://doi.org/10.1039/d0lc00974a>.
- [185] Omidian H, Rocca JG, Park K. Elastic, Superporous Hydrogel Hybrids of Polyacrylamide and Sodium Alginate. *Macromol Biosci* 2006;6:703–10. <https://doi.org/doi:10.1002/mabi.200600062>.
- [186] Langlois V, Trinh VH, Lusso C, Perrot C, Chateau X, Khidas Y, et al. Permeability of solid foam: Effect of pore connections. *Phys Rev E* 2018. <https://doi.org/10.1103/PhysRevE.97.053111>.
- [187] Deleurence R, Saison T, Lequeux F, Monteux C. Time scales for drainage and imbibition in gellified foams: Application to decontamination processes. *Soft Matter* 2015;11:7032–7.

<https://doi.org/10.1039/c5sm01158b>.

- [188] Lesov I, Tcholakova S, Denkov N. Factors controlling the formation and stability of foams used as precursors of porous materials. *J Colloid Interface Sci* 2014;426:9–21.  
<https://doi.org/http://dx.doi.org/10.1016/j.jcis.2014.03.067>.
- [189] Poulard C, Levannier S, Gryson A, Ranft M, Drenckhan W. Structuring Solid Surfaces with Bubble Coatings. *Adv Eng Mater* 2017;19.
- [190] Zabiegaj D, Santini E, Ferrari M, Liggieri L, Ravera F. Carbon based porous materials from particle stabilized wet foams. *Colloids Surfaces A Physicochem Eng Asp* 2015.  
<https://doi.org/10.1016/j.colsurfa.2015.02.031>.
- [191] Wintzenrieth F. Propagation du Son et Diffusion de la Lumière dans les mousses. Université Pierre et Marie Curie - Paris VI; 2015.